Project Report of Master of Engineering

Causes and countermeasures for crosstalk between the digital radiography high-voltage cable and the adjacent signal cable

디지털 엑스선 장비의 고압 케이블과 인접 신호 케이블간 Crosstalk 원인 및 대책

BY

PARK Taewook

FEBRUARY 2021

DEPARTMENT OF ENGINEERING PRACTICE
GRADUATE SCHOOL OF ENGINEERING PRACTICE
SEOUL NATIONAL UNIVERSITY

Project Report of Master of Engineering

Causes and countermeasures for crosstalk between the digital radiography high-voltage cable and the adjacent signal cable

디지털 엑스선 장비의 고압 케이블과 인접 신호 케이블간 Crosstalk 원인 및 대책

BY

PARK Taewook

FEBRUARY 2021

DEPARTMENT OF ENGINEERING PRACTICE
GRADUATE SCHOOL OF ENGINEERING PRACTICE
SEOUL NATIONAL UNIVERSITY

Causes and countermeasures for crosstalk between the digital radiography high voltage cable and the adjacent signal cable

NAM Sangwook

Submitting a Master's Project Report

FEBRUARY 2021

GRADUATE SCHOOL OF ENGINEERING PRACTICE
SEOUL NATIONAL UNIVERSITY

DEPARTMENT OF ENGINEERING PRACTICE

PARK Taewook

Confirming a Master's Project Report written
by
PARK Taewook

FEBRUARY 2021

Chair	KIM Seongwoo	(Seal)
Examiner	NAM Sangwook	(Seal)
Examiner	OH Jungsuek	(Seal)

Abstract

The term medical equipment refers to the devices used for disease prevention, diagnosis, and treatment of humans or animals. These types of equipment are different from general electronic devices in terms of their intended purposes of use. This means that it is more important to diagnose and treat accurately and quickly rather than use superior performance or cutting-edge technologies. Clearly, the application of the latest technologies that emerge following advancements in the information technology industry cannot be ignored, but the stability and reliability of products are separate issues.

Digital radiography (DR) is a system that consists of numerous circuits, cables, and electronic components. Because of its large scale and very complex structure, DR can potentially degrade the performance or damage other electronic devices owing to electromagnetic interference (EMI). In particular, noise mixed in high-voltage pulses for X-ray sources generated by the high-voltage generator (HVG) will propagates throughout the system, and cause EMI problems and malfunctions. Therefore, electromagnetic compatibility (EMC) for medical equipment products is a field directly related to product reliability.

This study analyzes the causes of noise generated by the HVG used in DR systems. In addition, we suggest a solution for EMI noise reduction. This EMI noise couples with an adjacent cable through a high-voltage cable.

Most of the EMI noise is reduced because the high-voltage cable in the DR system is shielded and has a high-optical coverage of 95%. However, as the amplitude of the X-ray pulse reaches several tens of kV and the receptor's load impedance is high enough in these typed of applications, it can be coupled to the adjacent signal cable and cause system malfunction.

Therefore, in this study, we analyze the mechanism of coupling in the shielded cable, and determine the cause of the noise source and the type of coupling using equivalent circuit analysis. As a countermeasure to noise, we propose a method that satisfies both low cost and high reliability.

keywords: Electromagnetic compatibility, Electromagnetic interference Digital radiography, Braided shield, Capacitive coupling, Inductive coupling, Crosstalk
student number: 2019-26941

Contents

List of Tables

List of Figures

Chapter 1

INTRODUCTION

It is very difficult to predict the electromagnetic interference/electromagnetic compatibility (EMI/EMC) phenomenon. is often difficult to even recognize that it is an EMC problem depending on the situation. In particular, digital radiography (DR) systems are vulnerable to EMI/EMC problems because of their very complex structure. In addition, the electromagnetic environment inside hospitals has become much more complicated in recent times compared with the past.

If the ground system is well designed at least, most of the EMC problems are not a big deal. However in the DR system, digital and analog circuits coexist and used cables are several tens of meters. So there is no ground system to be considered the correct answer. Therefore, the individual engineer's ability to solve the complicated EMC problems that arises would have a great influence on the results. In other words, even if you are an inexperienced EMC engineer, it will be able to approach problem solving more easily if you can simplify a complex system and know what the main cause of the problem is.

The purpose of this study is to simplify the huge system of the DR and to find out where the points that create the greatest noise and what its countermeasures can be.

1.1 Background

1.1.1 Digital Radiography System

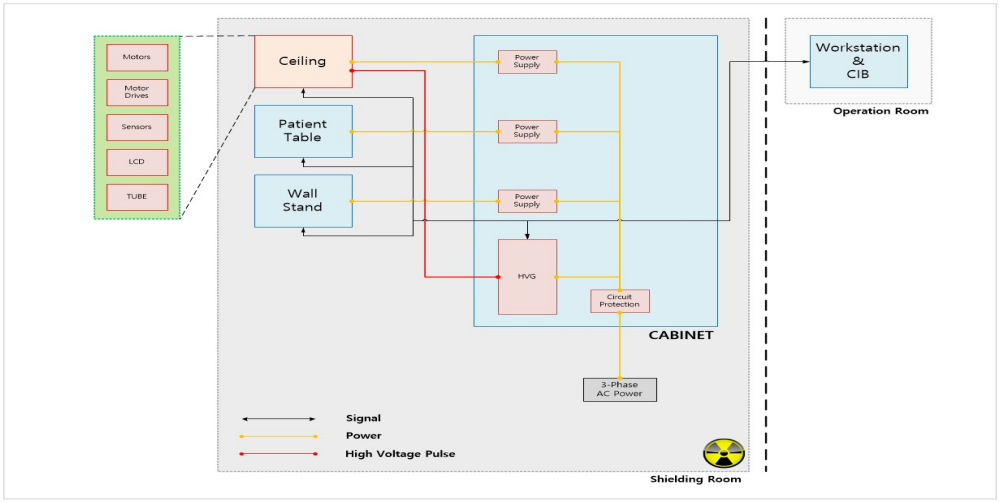

Figure 1.1: Block diagram of a digital radiography (DR) system.

X-ray has evolved a lot since it was discovered by Roentgen in 1850. Currently, most of the X-ray equipment used in the radiology departments are digital system. By applying the full-auto system, it is possible to move and operate the equipment without exerting great effort, and many technologies have been applied in terms of image quality improvement and ease of use. As a result, there are motors, motor drives, LCD, encoders, and sensors in the DR system, and various communication standards are used according to the application. Most of these components operate at the same time, and they have different purposes, so it is very difficult to find the cause of the problem with only visible symptoms.

The DR system mentioned in this study is a ceiling mounted type and is predominantly divided into the ceiling, the stand, the table, and the cabinet module. To briefly mention the role of the each module, the ceiling is a part that emits X-rays. The tube, which is an X-ray source, is located on the ceiling and is connected to the high-

voltage generator (HVG) through a high-voltage cable. It consists of an LCD monitor that informs the state of the equipment, parts for fully automatic operation, collision avoidance sensors, and a collimator that controls X-ray dose. And the stand and the table are parts that receive X-rays. They are used differently depending on the patient's positioning. Like the ceiling, there is a driving part and a detector that processes X-ray images. Lastly, the cabinet distributes power to each module. It also contains the HVG to generate high-voltage pulse for X-ray.

1.1.2 High-voltage Generator

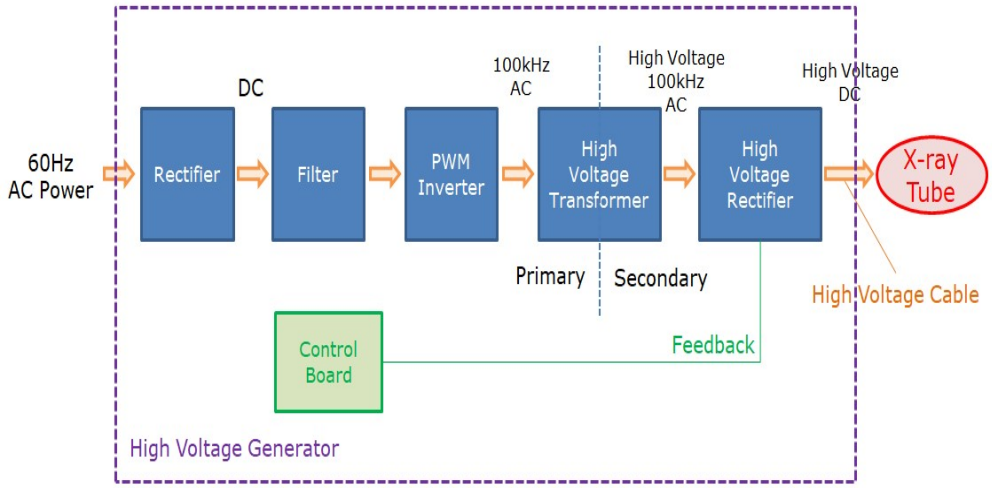

Figure 1.2: Schematic of the high-voltage generator (HVG).

The HVG generates high-voltage pulses for X-ray exposure, and functions to prevent unnecessary radiation exposure by monitoring the status of related modules. 50 to 60Hz AC single-phase or three-phase power is rectified with a rectangular type of tens of kV DC voltage and supplied to the tube. The HVG consists of the power distribution, the inverter, and the high-voltage Tank, roughly. In the power distribution, the AC voltage converts to the DC voltage by a rectifier circuit, The inverter is the FET full-bridge circuit using a PWM signal. It converts the DC into high-frequency AC. In

the HV Tank, there are boost transformer and voltage doubler circuit, high-voltage is generated. In the output, the anode voltage and the cathode voltage are combined to create the required voltage level.

Transformer

The performance of the HVG is depend on a transformer. Because of its size, efficiency, and reliability. Power elements such as transformers have a large difference between theory and practice in design. Therefore, a lot of trial and error is required for design. In terms of X-ray system performance, the ratio of the power output to the power input, power factor, loss, etc. will be important. However, it is very important to remove parasitic components that can act as a noise path at an operating frequency when it comes to the EMI noise. Since the voltage of several hundred V is raised to tens of kV, the degree of damage can be serious if high-frequency noise passes from the primary side to the secondary side of the transformer.

PWM inverter

As operating frequency of the HVG in a DR system goes up to several hundred kHz, PWM inverters are being used. Basically, an PWM inverter produces an AC pulse from a DC input by Pulse Width Modulation. The PWM inverter is commonly used for AC motor control purposes. As the operating frequency of the power electronics field is increasing in recent years, the switching speed of the inverter is also increased, and the voltage spike that occurs when the inverter is turned on or off is often a problem. This problem can also be a problem in a DR system. Since the output line of the inverter is long, ringing may be worse due to the line impedance.

1.1.3 High-voltage Cable

Figure 1.3 shows the high-voltage cable used for the DR system. The DR high-voltage cable satisfies the standard (IEC 60526 [1]) for “High-voltage cable plug and

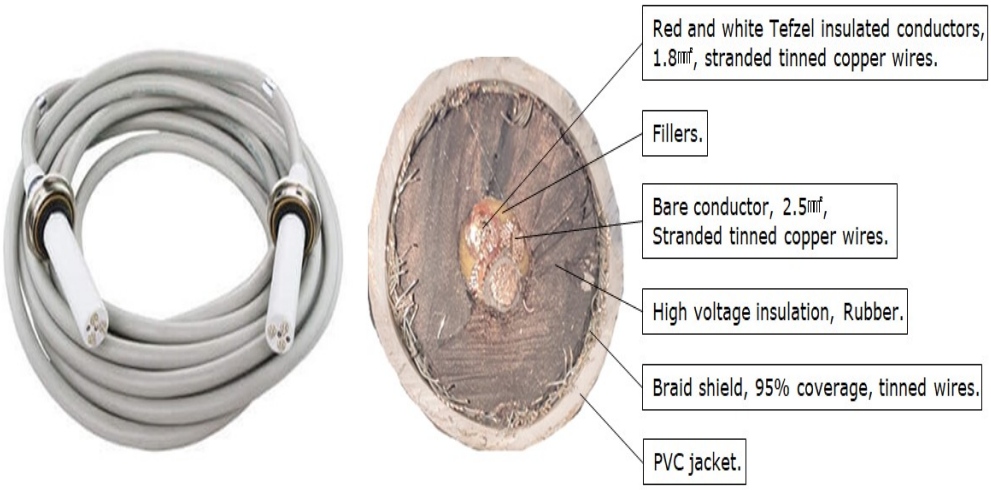

Figure 1.3: X-ray high-voltage Cable.

socket connections for medical X-ray equipment". As it acts as a path through which high power pulse is transmitted, it has a braided-shield structure with high shielding performance and a voltage rating of approximately $100\,\mathrm{kV}$. The internal structure is slightly different from the general coaxial cable, but there is only an additional filament line for heating the tube, so the overall structure is almost the same as the general coaxial cable. The DR high-voltage cable consists of two lines, the cathode line and the anode line. Each of the two lines is connected from the HVG to the tube, and plus voltage and minus voltage are applied. The filament line is only used for cathode cables for tube heating purposes. In this study, only the anode line is considered. Based on the DR system, since it starts from the HVG and connects to the tube in the ceiling, power cables and analog/digital signal cables are placed along the path, so it can operate as a noise transmission path.

1.2 Motivation

A shot noise referred to by X-ray developers refers to the noise that spreads throughout the system through cables at the timing of X-ray exposure, causing mal-

function of equipment or deterioration of image quality. It affects the whole system, and tendency is depend on state of cable wiring, equipment assembly, and environment. Most of the latest ceiling mounted equipment are full auto systems operated by remote control. In the situation when the patient is located, all moving parts should be stopped and only X-ray exposure should be performed. Unintended motion of the moving part is likely to lead to patient injury. In addition, if the image quality is degraded due to the noise, it is inevitable to retake. In particular, unnecessary radiation exposure to the elderly, children and pregnant women is a very serious issue.

Since the shot noise can bring serious side effects, there are a lot of efforts to reduce the shot noise. In order to present an accurate solution, it is necessary to know the cause, frequency and amplitude of the noise. However, analysis is very difficult due to the high complexity of the DR system. Solving EMC problems in complex systems starts from the stage of identifying symptoms and predicting the cause. However, the symptoms of shot noise are so irregular, and it is difficult to determine the frequency of the waveform seen through measurement. For these reasons, industrial sites often use expensive shielding cables to solve the problem. As price competition in the DR market is getting fiercer day by day, need an alternative which secure quality at a lower price. The key to solving EMC problems is to simplify the complex so that it looks simple. In this study, a huge DR system is abstracted into a simple equivalent circuit to analyze the causes and components of shot noise, and to validate the results through actual measurement and simulation.

Chapter 2

THEORETICAL BACKGROUND

As mentioned in the previous chapter, the high-voltage cable is a long cable that transmits the largest power in the DR system, so it can operate like an efficient antenna depending on the situation. Therefore, if the high-voltage cable acts as a noise path, it can cause problems throughout the whole system. Electromagnetic interference between a high-voltage cable and adjacent cables is called the crosstalk. The Crosstalk between the cables can be expressed into two types: the capacitive coupling and the inductive coupling. There is also the effect of conduction in terms of noise, but the effect is insignificant, so this study deals only the capacitive coupling and the inductive coupling when it comes to the crosstalk.

2.1 Coupling Mechanism

2.1.1 Capacitive Coupling

The capacitive coupling between two parallel non-shield type conductors in the low-frequency region can be expressed as a simple equivalent circuit, as shown in Figure 2.1. C_{gg} and C_{rr} are self capacitance of the generator and the receptor, respectively. C_{gr} is a mutual capacitance that exists between the generator and the receptor. R is a termination resistance of both ends of the receptor, which is determined by what

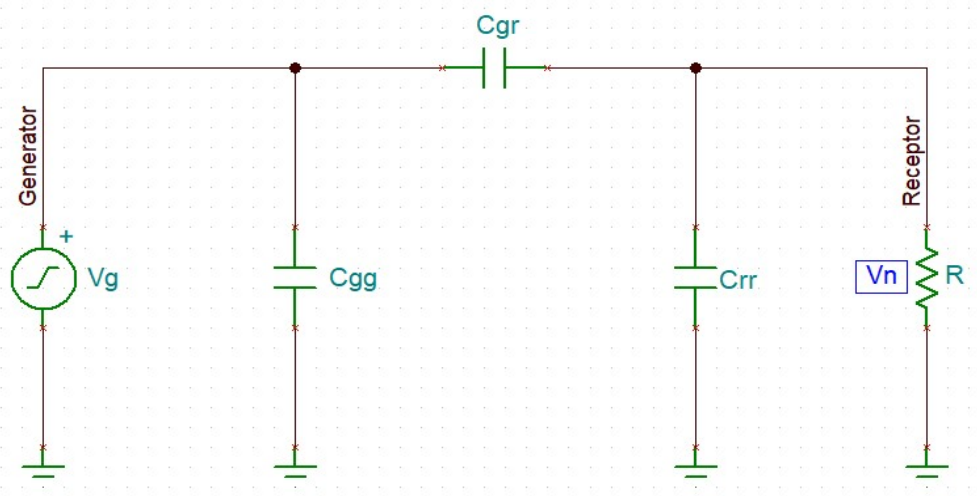

Figure 2.1: Equivalent circuit of the capacitive coupling between two non-shield wires.

is the load of receptor circuit. Value of R is several $\mathrm{k}\Omega\sim$ tens of $\mathrm{k}\Omega$ in common usage. Finally, V_n is the noise voltage seen as a result of noise coupling between the two conductors. V_n is expressed as these lumped parameters as follows.

$$V_n = V_{FE}^{CAP} = V_g \times \frac{\frac{j\omega C_{gr}}{C_{gr}+C_{rr}}}{j\omega + \frac{1}{R(C_{gr}+C_{rr})}}. \tag{2.1}$$

In most cases, R is less than the combined impedance of C_{gr} and C_{rr} ($0.1\,\mathrm{nF}$ level based on a 2mm diameter conductor), so Equation (2.1) can be simplified as follows [2].

$$V_n = V_{FE}^{CAP} = V_g \times j\omega RC_{gr}. \tag{2.2}$$

Based on Equation (2.1), the coupling between 2mm diameter non-shielded wires is measured and simulated. At this time, R is $5\,\mathrm{k}\Omega$ for composite impedance of both Receptor near-end (NE) and far-end (FE), and 6AWG ground wire is placed side by side along with the generator and the receptor to work as a reliable ground. Source was applied 5V single-tone sine wave using an arbitrary waveform generator (AWG), as shown in Figure 2.2 and Figure 2.3. As a result of the measurement, the coupling is

approximately 2 V, and the cut-off frequency is approximately 800 kHz, and saturation occurs in the higher frequency region.

Table 2.1: Setup parameters of non-shielded case.

Parameter	Variable	Value	Units
Length	l	1	m
Height above ground	h	0	m
Diameter of cable	dwg, dwr	2	mm
Separation	s	touching	-
Load impedance	Z_{FE}, Z_{NE}	10	kΩ

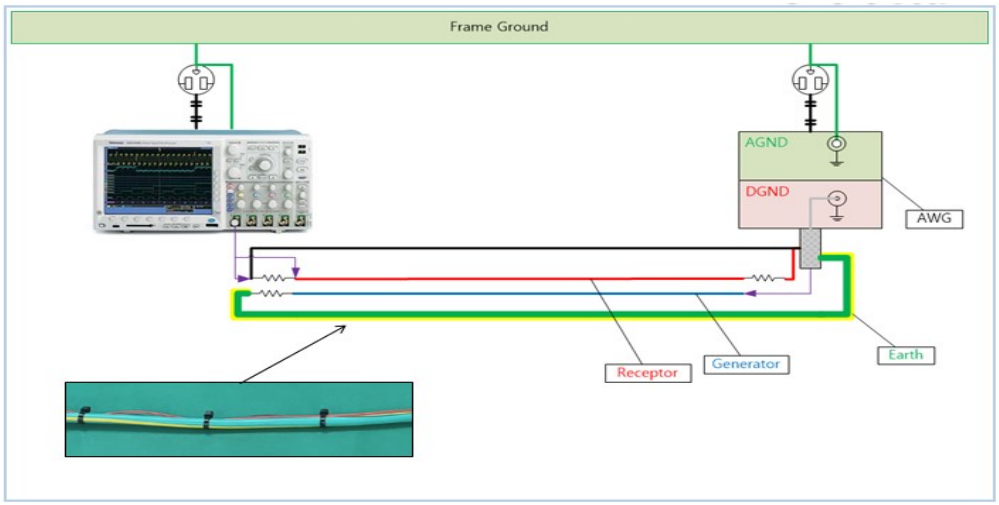

Figure 2.2: Block diagram of two non-shielded wires case.

2.1.2 Inductive Coupling

When the current I_g flows through the conductor, magnetic flux Φ is generated in proportion to this, and the proportional constant between the two is an inductance. With this logic, a mutual inductance can be defined when a current flows through the

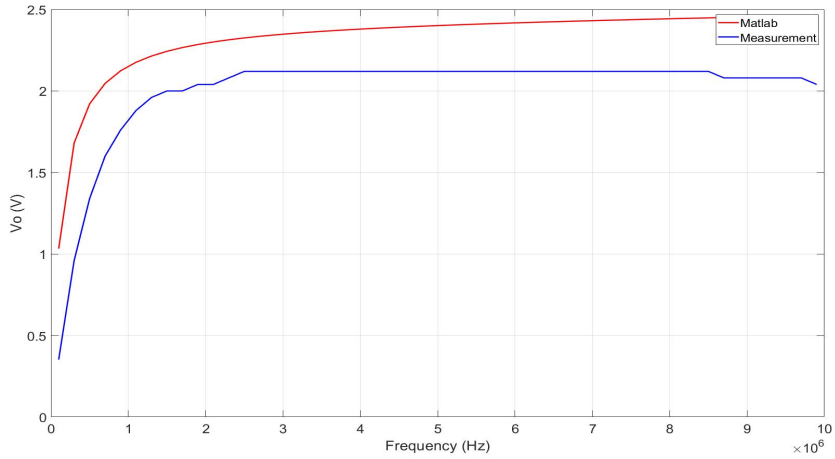

Figure 2.3: Frequency response of the capacitive coupling between two non-shielded wires.

circuit of the generator and a magnetic flux is generated in the receptor [2]. Therefore, it can be expressed as a simple circuit is shown in Figure 2.4. Also, V_n caused by the influence of inductive coupling is as shown in Equation (2.3).

$$V_n = V_{FE}^{IND} = I_g \times j\omega L_{gr}. \tag{2.3}$$

From Equation (2.3), it can be observed that the noise can be reduced only when the mutual inductance (L_{gr}) is small. Since R is much larger than $j\omega L_{gr}$ (approximately $300\,\mathrm{nH}$ for a $2\,\mathrm{mm}$ diameter lead), it can be predicted that the inductive coupling will have less effect.

The capacitive coupling and the inductive coupling appear in parallel and series based on V_n in the receptor circuit. Therefore, in the case of inductive coupling, V_n at FE has a phase difference of 180° from the source, and V_n at NE has the same phase as the source. Figure 2.5 is the result of applying a rectangular pulse of size $5\,\mathrm{V}$, width $10\,\mu\mathrm{s}$, and rising/falling time $10\,\mathrm{ns}$ to the above structure. The phases of NE and FE are consistent, and this result indicates that the capacitive coupling is dominant in this

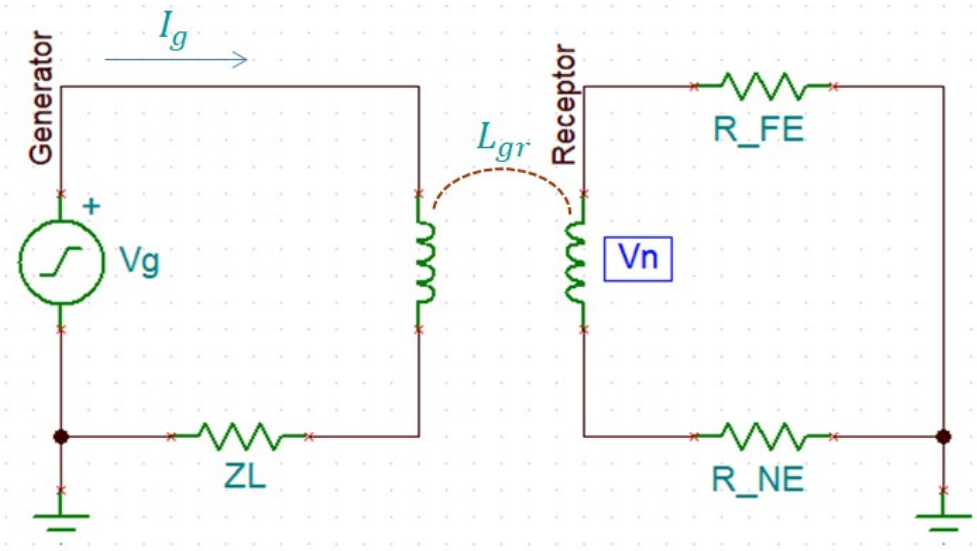

Figure 2.4: Equivalent circuit of the inductive coupling between two non-shielded wires.

structure.

There are a number of factors that influence the coupling result, such as voltage and current, load impedance, and mutual elements. Especially, L_{gr} is related to the area created by the receptor circuit loop. Since the generator, the receptor, and the ground circuit are completely in close contact with each other, so the influence of L_{gr} inevitably decreases. In addition, as mentioned above, since the coupling voltage at the receptor by inductive coupling is in series with line. According to the voltage distribution law, inductive coupling effect would be decrease, because the impedance of FE and NE are very large.

As for the DR high-voltage cable and signal cable to be covered in this study, the termination impedance is $10\,\mathrm{k}\Omega$ and the distance between cables is 0, so it can be expected that the capacitive coupling will be dominant.

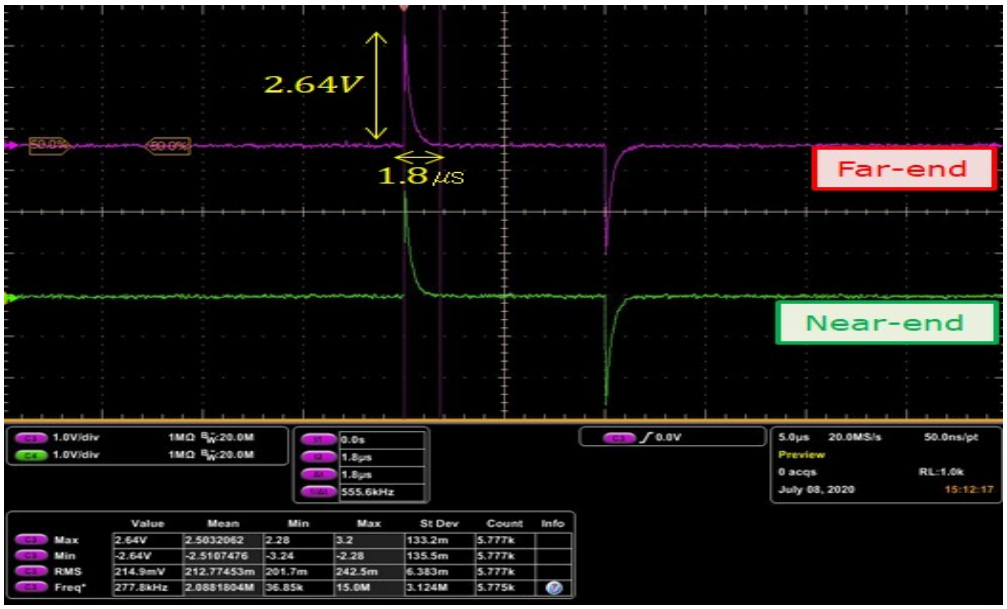

Figure 2.5: Measurement of coupling between two non-shielded wires applied rectangular pulse.

2.2 Effect of Shield

For EMC engineer, electromagnetic shielding is just one method in a quite impressive “arsenal” of EMI mitigation techniques [3]. Again, this implies that shielding is an accessible and effective way to solve EMI problems, but it is not always best solution. Even in real-world problems, when interference occurs in a cable due to unknown noise, it is often solved by just shielding. However, it is not correct to approach shielding as a troubleshooting method from the start. Shielding is the last thing to approach after considering many conditions such as, what is the noise to be removed through shielding, how to terminate the shield conductor, are there any cost issues. Shielding the cable without the analysis of the coupling mechanism may cause adverse effects. For instance, if the cause of the problem is the inductive coupling, the grounding of both ends of the shield rather provides a wide loop and the result may be worse.

Before discussing cable shielding, it should be noted that the shielding structure

applicable to the cable is limited. The first complete shielding structure that can be considered is a solid. However, considering the curvature of the cable, the solid structure is not appropriate. Therefore, the shielding structure applied to the cable is usually divided into three types: a spiral, a braid, and a foil.

The spiral shielding is used for cables because of its low manufacturing cost, excellent flexibility, and easy termination [2] [3]. The shielding effect is given by winding the wire in the form of a strip along the axis direction of the cable.

The braided shielding is a form in which the spiral shielding is wound one more time in the opposite direction, and has a shielding effect of approximately 60 to 98% compared to the normal solid structure [2] [3]. It is more expensive to manufacture than the spiral and its flexibility is a little worse, but it is widely used for cables due to its excellent shielding performance.

Lastly, the foil shielding has an E-field shielding effect that is almost equivalent to that of the solid structure, but there may be problems in terms of durability. The difference in performance for each structure is compared through transfer parameters, which are good indicators for the cable shielding effect in Chapter 2.2.2.

2.2.1 Structure of the Braided Shield

The DR high-voltage cable targeted by this study has the braided shield structure. As mentioned above, it is a structure in which several strands of wire are woven in a net form to surround the inner conductor. DR HV cable has 95% Optical coverage, as mentioned in the Spec sheet. This means that there are some open spaces, and you can see that fields can leak through these apertures. The coupling mechanism that usually occurs between the external electromagnetic field and the inner conductor of the coaxial cable is as follows [4].

1. Diffusion of the E and H fields through the sheath material

2. Penetration of the fields through the small apertures of the braided shields

3. A more complicated induction phenomenon due to overlapping of the individual strands of the shield

This study deals with the braided shield, but the area where the wire and wire overlap is considered as one conductor and focuses on the effect of the field exiting through the open area, so case 3 is not considered. Figure 2.6 shows the shield structure of the DR high-voltage cable.

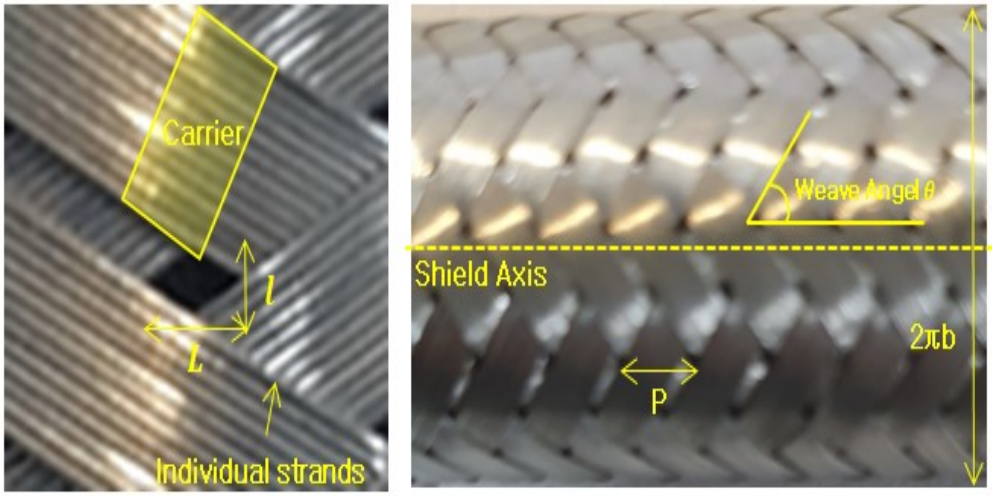

Figure 2.6: Structure of the high-voltage cable's braided shield of the DR system.

The main parameters representing the braided shield are as follows. N (the number of strands in each carrier), d (strand wire diameter), C (the number of carriers), b (shield radius), Θ (weave angle), K (the optical coverage, F (the fill factor). Each parameter is not independent and has a relationship in Equation (2.4), which greatly affects the shield structure and performance.

$$F = \frac{NCd}{4\pi a \cos\Theta}. \tag{2.4}$$

$$K = 2F - F^2. \tag{2.5}$$

The indicator of the shielding performance is the optical coverage, and the effect of the parameter variation on the optical coverage based on the structure of the DR

high-voltage cable ($N = 12$, $d = 0.12\,\mathrm{mm}$, $C = 24$, $b = 7.35\,\mathrm{mm}$, $\Theta = 72°$) is shown in Figure 2.7.

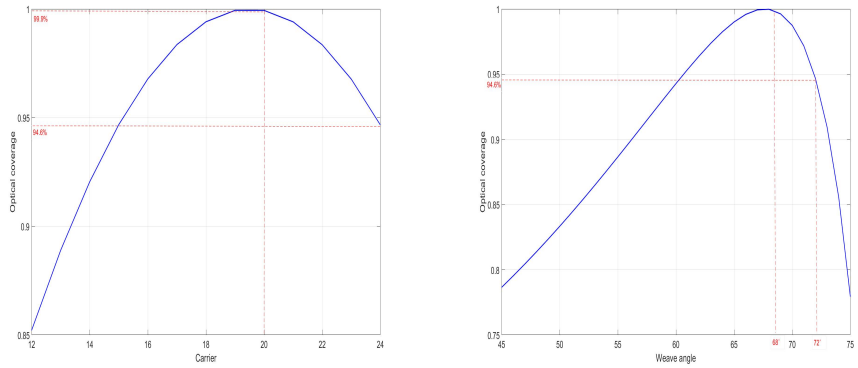

(a) (b)

Figure 2.7: (a) Optical coverage and Carrier. (b) Optical coverage and Weave angle.

Figure 2.7(a) shows the variation of the optical coverage with the number of carriers. Since the shield structure has 24 carriers, it has a coverage performance of approximately 94.6%, but it can be observed that the highest coverage can be secured when there are 20. However, there is a cable flexibility problem, so coverage up to 99% is not used in common usage. Figure 2.7b shows the variation of the optical coverage with the weave angle. As the angle increases in the direction of the shield's axis, the Optical coverage improves, the highest coverage is approximately 68°, and the actual structure shows 94.6% performance at 72°.

2.2.2 Transfer Parameter

Coupling analysis occurring in a cable with braided shield structure can be expressed as the transfer impedance and the transfer admittance. This is an approximation of the coupling phenomenon through the rhombus-shaped aperture of the braided shield by using electric and magnetic polarizabilities of the elliptical-shaped aperture of similar size [5]. In particular, the transfer impedance is good to use as an indicator

for evaluating the characteristics of the shield. The general form is expressed as the ratio of the open circuit voltage of the inner conductor of the coaxial cable and the shield current.

$$Z_t = \frac{1}{I_s}\frac{d\mathrm{V}}{dl}. \tag{2.6}$$

Where Z_t is the transfer impedance (Ω/m), Is is the shield current, V is the induced voltage between the inner conductor and the shield conductor, and l is the length of the cable.

The transfer impedance for the braided shield structure is expressed as a diffusion term and a penetration term, and the form is as follows [4] [5].

$$Z_t = Z_d + j\omega L, \tag{2.7}$$

$$Z_d = \frac{4}{\pi d^2 NC\sigma\cos\Theta}\frac{(1+j)\frac{d}{\delta}}{\sinh(1+j)\frac{d}{\delta}}, \quad [\Omega/\mathrm{m}] \tag{2.8}$$

$$L = \frac{\pi\mu_0}{6C}(1-K)^{\frac{3}{2}}\frac{e^2}{E(e)-(1-e^2)K(e)} \quad (for\,\Theta < 45^\circ), \quad [\mathrm{H/m}] \tag{2.9}$$

$$L = \frac{\pi\mu_0}{6C}(1-K)^{\frac{3}{2}}\frac{\frac{e^2}{\sqrt{1-e^2}}}{E(e)-(1-e^2)K(e)} \quad (for\,\Theta > 45^\circ). \quad [\mathrm{H/m}] \tag{2.9a}$$

Where $E(e)$ and $K(e)$ are the first and the second kind complete elliptic integral functions, and e is the eccentricity of the elliptical aperture.

$$l_{eq} = L_{eq}\tan\Theta \qquad (for\,\Theta < 45^\circ), \tag{2.10}$$

$$l_{eq} = L_{eq}\cot\Theta \qquad (for\,\Theta > 45^\circ), \tag{2.10a}$$

$$e = \sqrt{1-(\frac{l_{eq}}{L_{eq}})^2}. \tag{2.11}$$

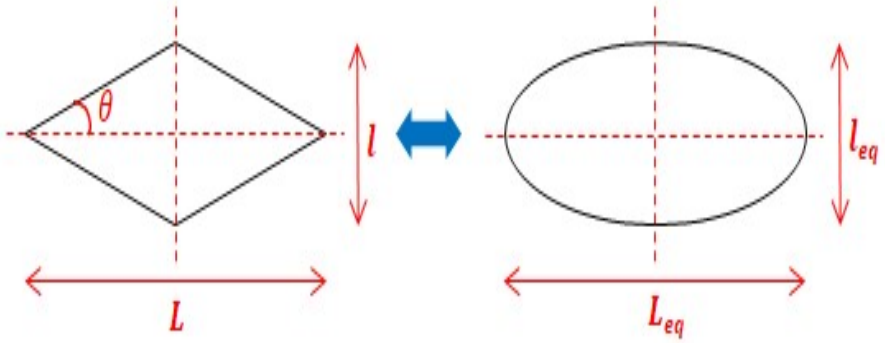

Figure 2.8: Approximation of the braided shield aperture.

The transfer admittance is a susceptance between the inner conductor and the return path of the shield current, and its general form is as follows.

$$Y_t = \frac{1}{V_s}\frac{dI}{dl}. \tag{2.12}$$

Where Y_t is the transfer admittance $(\mathrm{S/m})$, V_s is the voltage between the shield and the current return path for the shield current, and I is the current of the inner conductor. The formula of transfer admittance for the braided shield structure is as follows [4] [5].

$$Y_t = \frac{j\omega\pi C_1 C_2}{6C\epsilon_0}(1-K)^{\frac{3}{2}}\frac{1}{E(e)} \qquad (for\,\Theta < 45^\circ), \quad [\mathrm{S/m}] \tag{2.13}$$

$$Y_t = \frac{j\omega\pi C_1 C_2}{6C\epsilon_0}(1-K)^{\frac{3}{2}}\frac{1}{1-(1-e^2)E(e)} \qquad (for\,\Theta > 45^\circ). \quad [\mathrm{S/m}] \tag{2.13a}$$

Shielding performance according to the shield structure examined using transfer parameters is shown in Figure 2.9. Y axis is absolute value of the transfer impedance. It shows the variation of transfer impedance with frequency in log scale. The smaller the transfer impedance, the better the shielding effect, and the larger the transfer impedance, the worse the shielding effect. In the low-frequency region below $100\,\mathrm{kHz}$, the diffusion term of the transfer impedance is dominant, and both of the solid structure and braid structure show very good shielding performance.

As frequency increases, the impedance of the solid and the braid decreases approximately $1\,\mathrm{MHz}$ due to the skin effect. Over $1\,\mathrm{MHz}$, electromagnetic field pene-

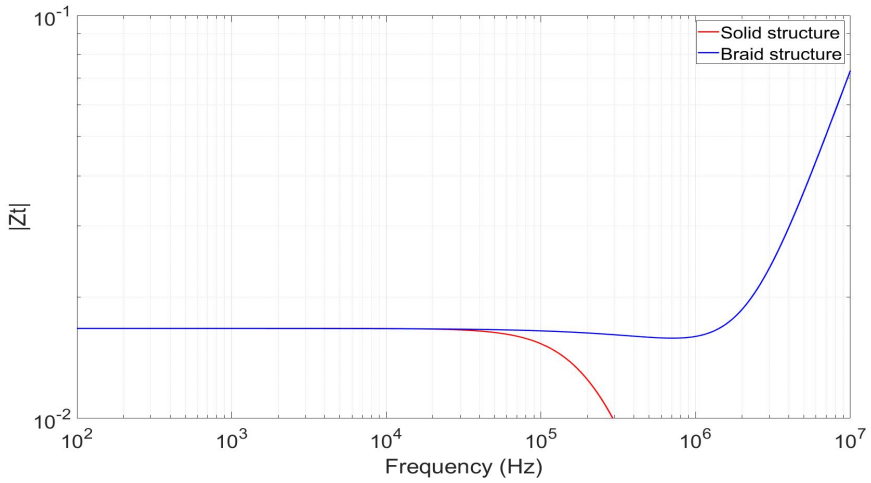

Figure 2.9: Transfer impedance according to the shielding structure.

trates into the aperture of the braided shield increasingly, unlike the solid. Also the impedance increases rapidly. Except the solid structure, the structure with the most outstanding shielding performance would be the multi layer braided shield, which is mainly used in communication cables (Cat. 7) that require Gbps speed. It satisfies both the flexibility of the braided shield and the shielding performance of the solid shield.

The following is the shielding performance according to the parameter sweep of the braided shield. It can be observed that the optical coverage variation and the braided shield performance variation with the number of carriers. Figure 2.10 and Figure 2.11 are the results of plotting based on the DR high-voltage cable structure, and it can be observed that the transfer parameter variation with the relationship between the number of carriers and the optical coverage.

Lastly, Figure 2.12 shows the transfer impedance of the DR high-voltage cable shield. It shows that the skin effect appears approximately 1 MHz, and the shield characteristics are poor at frequency over 1 MHz. As described above, field penetrates through the braid shield aperture over 1 MHz, so that the shielding performance is degraded and the coupling level may increase.

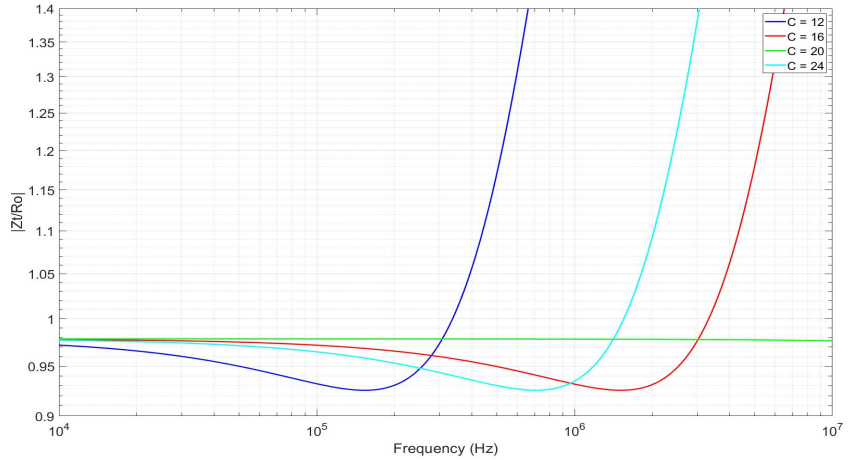

Figure 2.10: Transfer impedance according to change Carrier.

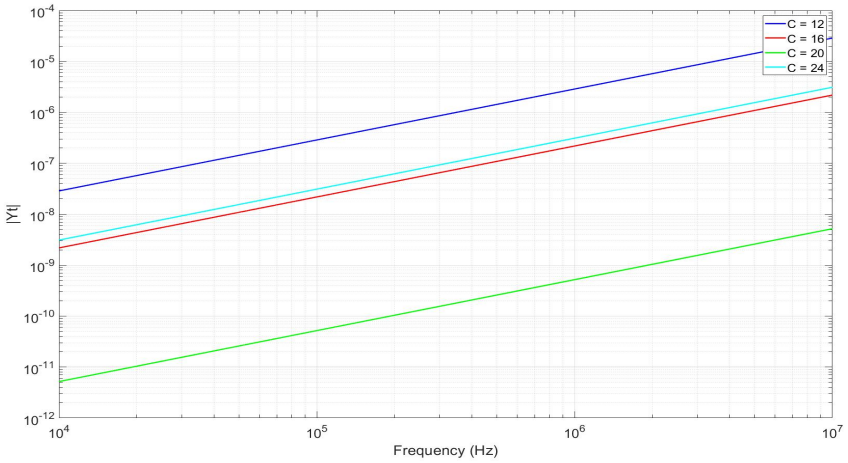

Figure 2.11: Transfer admittance according to change Carrier.

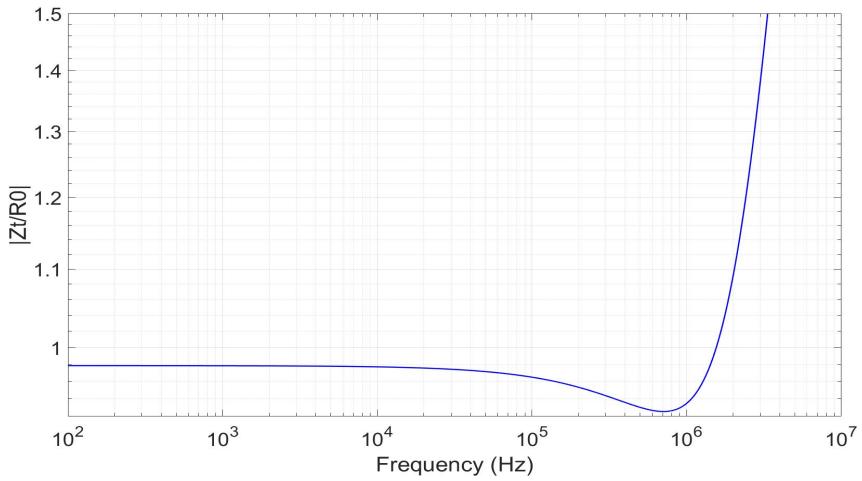

Figure 2.12: Transfer impedance of the high-voltage cable of the DR system.

2.2.3 Effect of the Shielding Condition

We examined how the shielding characteristics vary depending on the shield structure. It is necessary to look at the variation of the coupling level when the shield is grounded and when it is not, and when the shield is damaged. It was stated earlier that the DR system is connected by a number of cables between the modules. In addition, since the DR is full-auto system using motors, cables used in the moving parts are placed in the cableveyor to ensure mobility. Before wiring in the cableveyor, it is necessary to consider the radius of curvature of each cable, the prevention of friction or twisting between cables, and classification according to the purpose or weight of the cables. The rules that must be observed when wiring in the cableveyor are as shown in Table 2.2. These rules are not absolute. There may be slight differences in the standards recommended for each maker.

Figure 2.13 shows an example of a cross-sectional view of the cableveyor with cables. In the case of the left side, the wiring rules were not observed at all. On the other hand, the right side is designed according to the wiring rules. In case of wiring as shown on the left, the outer shell of the cable is gradually peeled off due to friction

Table 2.2: Rules of wiring in the cable veyor

Rules	Contents
Filling rate	Do not fill more than 80% of cross-sectional area
Clearance	Provide free space for 10% of cable diameter in all directions
Separation	Separate according to cable diameter and application
Radius of curvature	Use cableveyor with curvature greater than cables

when the equipment is moving, and eventually the inner conductor may be damaged. On the contrary, the right side can be used without problems for much longer time than the left side. However, there is a trade-off. Product stability is important for the medical equipment such as DR, but design is as important as it is, so it is impossible to design the product ignoring the product size as shown on the right. Therefore, design should be considered while keeping the rules as much as possible.

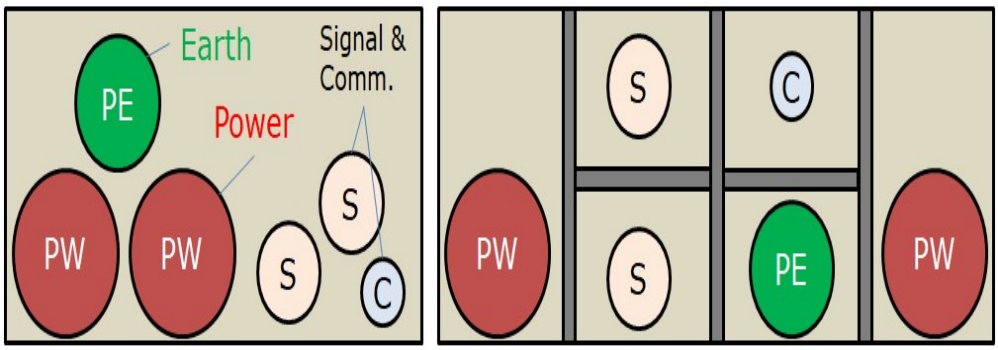

Figure 2.13: Example of wiring in cableveyor.

Well-grounded shield

First, look at the case when the cable shield is well grounded. The coupling level can be calculated using the coupling mechanism mentioned in the non-shield case and

transfer parameter.

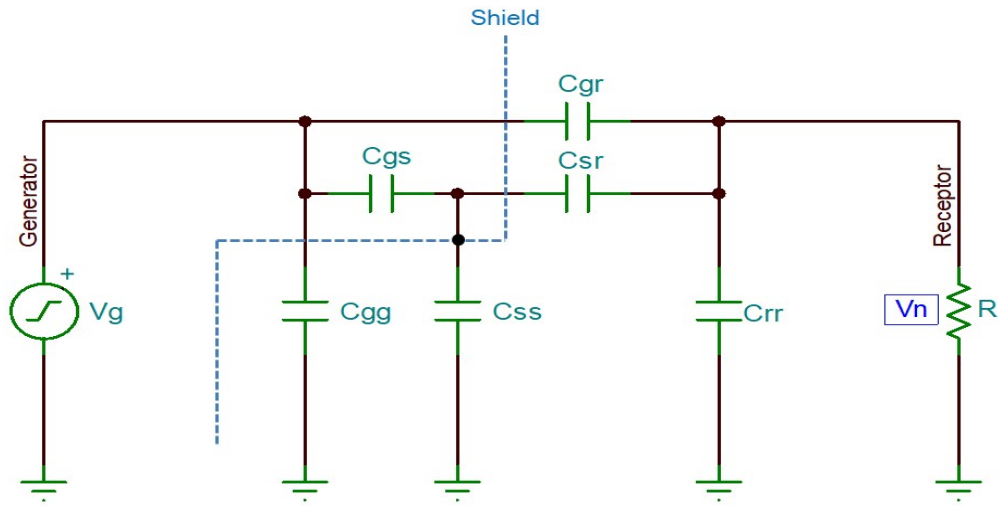

Figure 2.14: Equivalent circuit of grounded braid shield.

Figure 2.14 shows an equivalent circuit model considering only the capacitive coupling. Since both ends of the shield of the generator are completely connected to the ground, the capacitance between the conductor inside the generator and the shield (C_{gs}), the capacitance between the receptor and the shield (C_{sr}), and the capacitance between the shield and the ground (C_{ss}) are all 0. Therefore, these parameters have no effect on the results. The remaining parameters are C_{gr}, C_{rr}, and R. C_{gr} is the mutual capacitance between the generator inner conductor and the receptor conductor. If the shield is a solid structure, the E field passing through will be 0, but as it is a braided shield, transfer admittance is applied in consideration of the component that penetrates through the aperture. The formula that summarizes V_{FE}^{CAP} in terms of V_g is as follows.

$$V_N = V_{FE}^{CAP} = V_g \times \frac{j\omega C_{gr} R}{1 + j\omega C_{rr} R + j\omega C_{gr} R}. \tag{2.14}$$

We measured and simulated based on the formula. The specifications of cable are as shown in Table 2.3. Source was applied 5V single-tone sine wave using the AWG. Due to the influence of the braid shield, the coupling level is too low to measure. Matlab simulation result is shown in Figure 2.15. The coupling level is approximately

$1\,\mathrm{mV}$ over $5\,\mathrm{MHz}$. Cut-off frequency is approximately $3\,\mathrm{MHz}$. Figure 2.16 shows the transfer impedance of this case. Y axis is the transfer impedance normalized with the DC resistance. It can be observed that the shielding performance is rapidly deteriorated from over $3\,\mathrm{MHz}$.

Table 2.3: Specifications of cables.

Parameter	Variable	Value	Units
Coupling length	cl	1	m
Height above ground	h	0	m
Diameter of generator	dwg	0.88	mm
Diameter of receptor	dwg	2	mm
Diameter of the shield	$dwsg$	3	mm
Separation	s	touching	-
Load impedance	Z_{FE}, Z_{NE}	10	kΩ
Weave angle	$theta$	30	°
Number of Carrier	C	16	ea
Number of strand wires	N	7	ea
Principal axis length of aperture	L	1	mm

Isolated shield

Next is the situation in which the ground of the shield is completely disconnected. The shielding cable used in the moving part can be damaged because the wiring rules are not properly followed. Equivalent circuit is the same as Figure 2.14. The difference from the well-grounded case is the capacitance related to the shield must be considered because the shield is not grounded. The formula summarized based on the equivalent

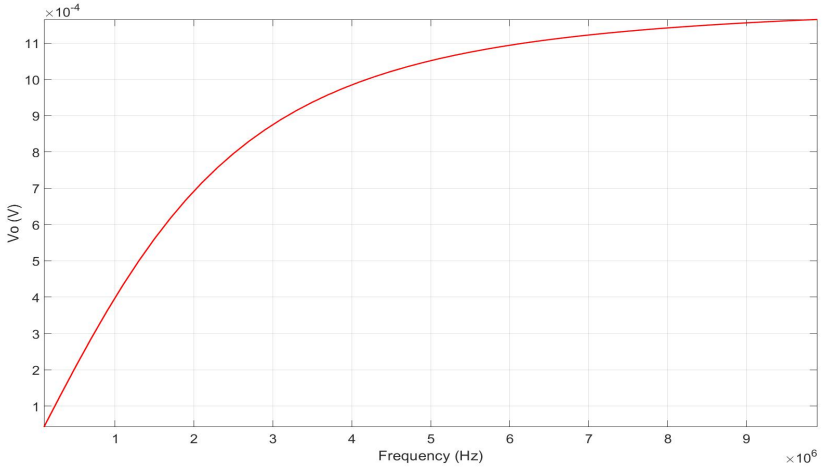

Figure 2.15: Frequency response of the capacitive coupling grounded braid shield case.

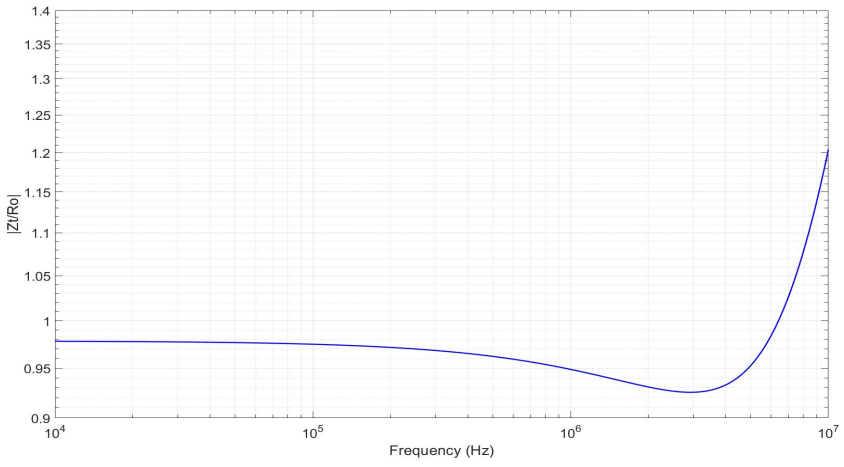

Figure 2.16: Transfer impedance of grounded braid shield case.

circuit is as follows. V_{SHIELD} is voltage on the shield.

$$V_{SHIELD} = V_g \times \frac{C_{gs}}{C_{gs} + C_{ss}}. \tag{2.15}$$

$$V_N = V_{FE}^{CAP} = V_{SHIELD} \times \frac{\dfrac{R}{1 + j\omega RC_{rr}}}{\dfrac{1}{j\omega C_{sr}} + \dfrac{R}{1 + j\omega RC_{rr}}}. \tag{2.16}$$

The measurement and simulation results are shown in Figure 2.17. Parameters for measurements are same with well-grounded case. Equation (2.16) is plotted by Matlab. The coupling level is approximately 1.7V, and it is almost similar to the non-shield case. This result indicates that the shielding effect is very poor if the shield is not well grounded, at least when the capacitive coupling is dominant.

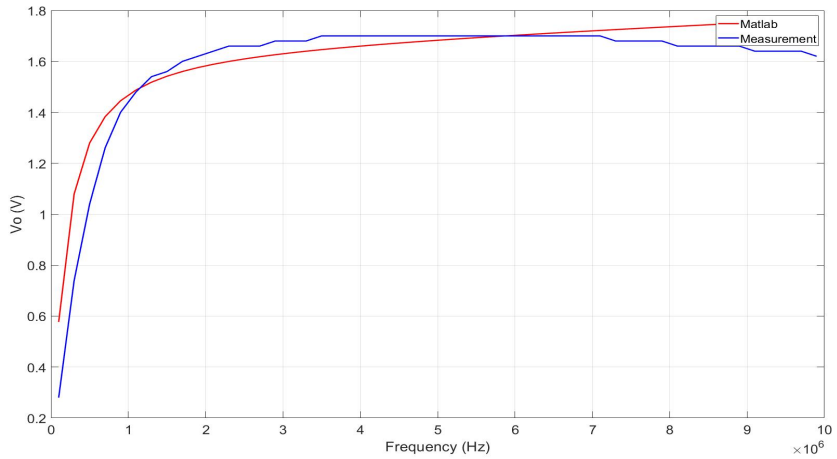

Figure 2.17: Frequency response of the capacitive coupling isolated braid shield case.

Interrupted shield

The following is a case where the shield is connected like a pigtail that is not completely disconnected. Mostly, when a problem occurs inside the cableveyor, the

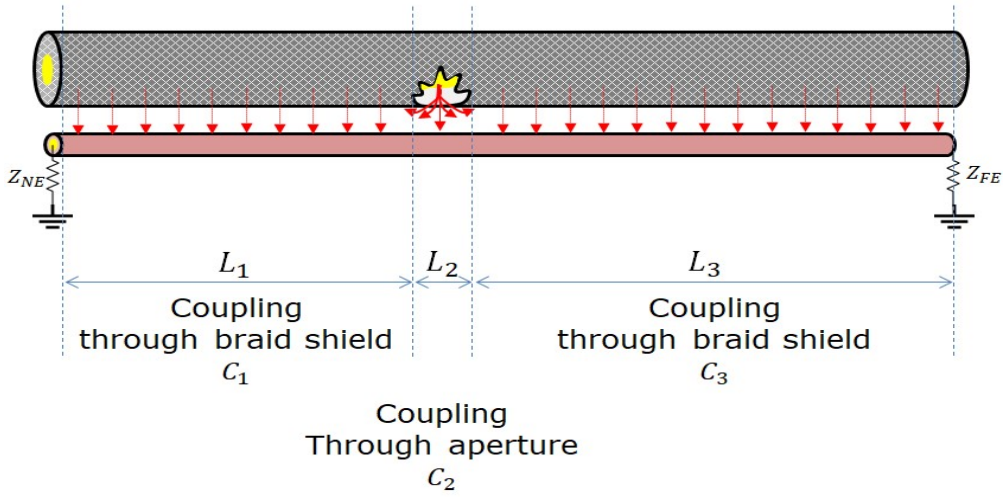

Figure 2.18: Interrupted shield case.

shield conductor has some interruption. In this case, there seems to be no problem with the open/short test since the conductor is not completely disconnected. However, the shielding effect is degraded, so the coupling noise increases. The coupling mechanism is not very different from the previous cases. However, it is important how to express the shield area attached only in the form of the pigtail. As shown in Figure 2.18, total coupling can be calculated by superimposing braided shield section and interrupted section. [6]

$$Coupling = (C_1L_1) + (C_1L_1) + (C_1L_1). \tag{2.17}$$

Figure 2.19 and 2.20 are comparison of the measurement and equivalent circuit results with the non-shield case. Since the shield is not completely cut off, the shielding effect remains. The y-axis represents the V_i over V_o as a log scale, and the x-axis is the log scale of the frequency. It is assumed that an aperture of approximately 8cm is formed, and it can be observed that the non-shield is approximately 10 times more coupled.

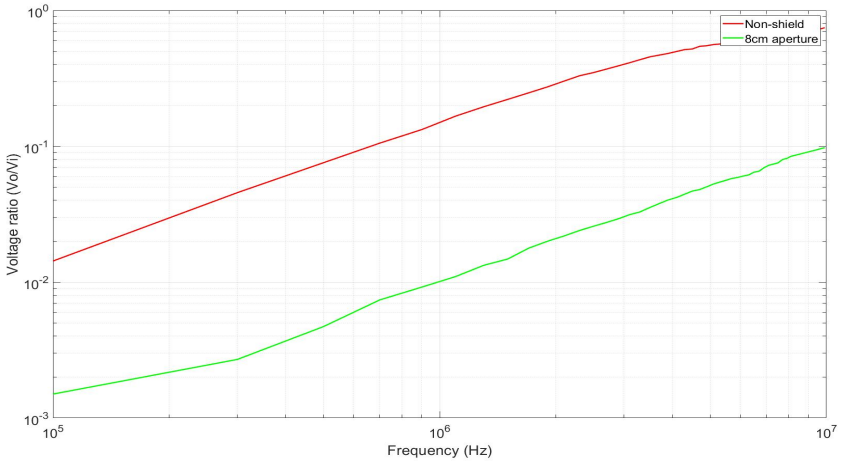

Figure 2.19: Measurement - Comparison with non-shield case.

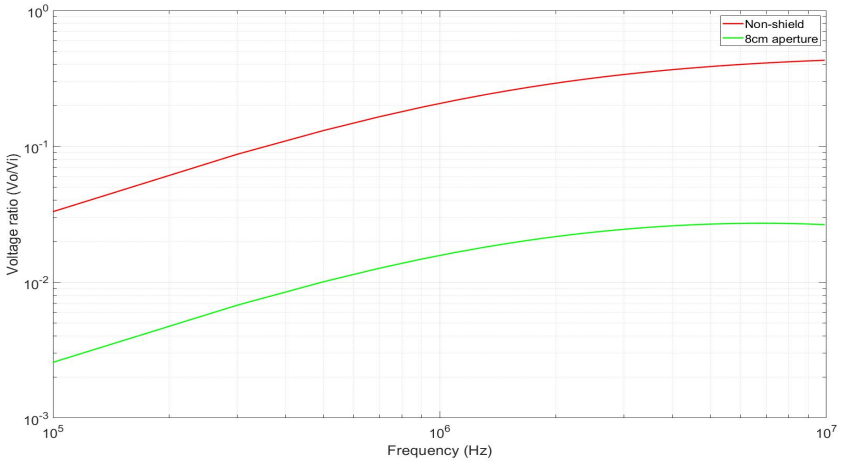

Figure 2.20: Matlab - Comparison with non-shield case.

2.3 Conduction Noise

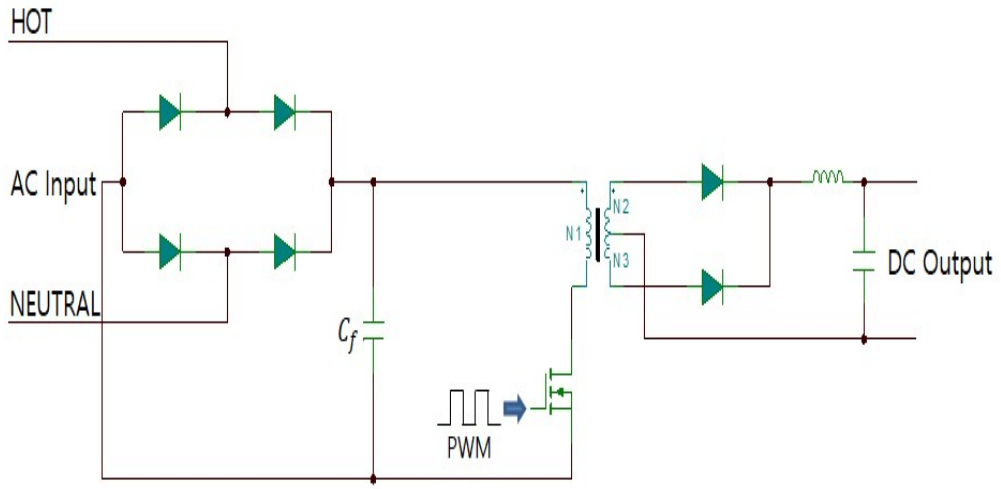

Figure 2.21: Flyback converter SMPS.

We will describe where the noise source that causes the crosstalk between the cables can occur. The DR HVG has similar structure and operation principle to the Switching Mode Power Supply (SMPS). Therefore, noise analysis generated in the HVG can also be approached in the same way as the SMPS. The SMPS is more than 85% efficiency and is widely used because of its small size and light weight. However, the demerit is also clear. It is the main source of both conducted and radiated emissions. Among them, we have to consider the conductive emission, which is again classified into the common-mode noise and the differential-mode noise.

Figure 2.21 shows a simple schematic of the flyback converter SMPS. The PWM controller operates the FET inverter, and the noises generated at this time can be conducted through several paths. In the case of common-mode noise, it is mainly conducted to the primary side or the secondary side through the parasitic capacitance generated by the SMPS structure. For the differential-mode noise, the filtering capacitor (C_f) in front of the PWM controller cannot function as a perfect filter due to internal ESL and ESR, so some noise returns to the bridge circuit. Therefore, in this study, only

the common-mode noise is considered because we are interested in noise that causes EMI problems by conducting through the high-voltage cable connected to the output of the HVG..

2.3.1 Common-mode Noise

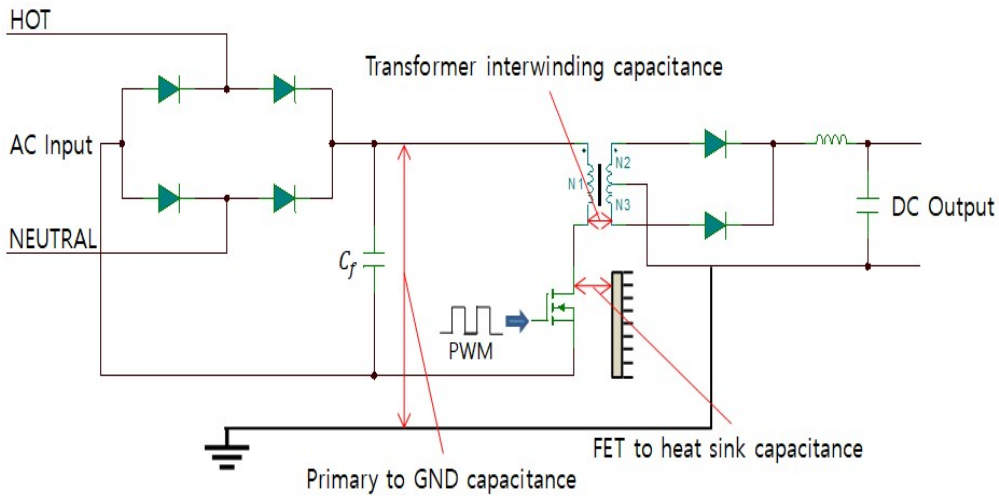

Figure 2.22: Parasitic capacitances of the SMPS.

As explained earlier, the common-mode noise is conducted through the parasitic capacitance. In H.Ott's EMC Engineering, the path of common-mode noise is divided into three [2].

1. Capacitance between FET and heat sink
2. Capacitance between the primary and the secondary sides of the transformer
3. Capacitance between the primary conductor and ground

The magnitude of the parasitic capacitance is known to be approximately $50\,\mathrm{pF}\sim500\,\mathrm{pF}$. The frequency must be quite high for the parasitic capacitance to work as a noise path. If we consider that the parasitic capacitance of approximately $500\,\mathrm{pF}$ and the terminal impedance of $\mathrm{k}\Omega$ level are similar to those of the high pass filter, noise above

the frequency of approximately 600 kHz can sufficiently pass. The HVG has a higher operating frequency than in the past, so the PWM controller operates at hundreds of kHz, but not enough to be called high-frequency. If ringing occurs during the PWM operation, its frequency reaches several tens of MHz, so it can operate as noise.

Solutions of the parasitic path problems are as follows. First, we can use an insulating washer between the FET and the heat sink. It blocks the noise path by isolating only the FET. Second, increasing the distance between the primary and secondary sides of the transformer. This means that by reducing the capacitance between the primary and secondary side, it will not act as a path. Lastly, isolating the heat sink from the ground. However, these solutions can create safety issues and there can be size issues. The role of blocking the noise path is clear, but the side effects are also clear.

2.3.2 Rectifier Diode Noise

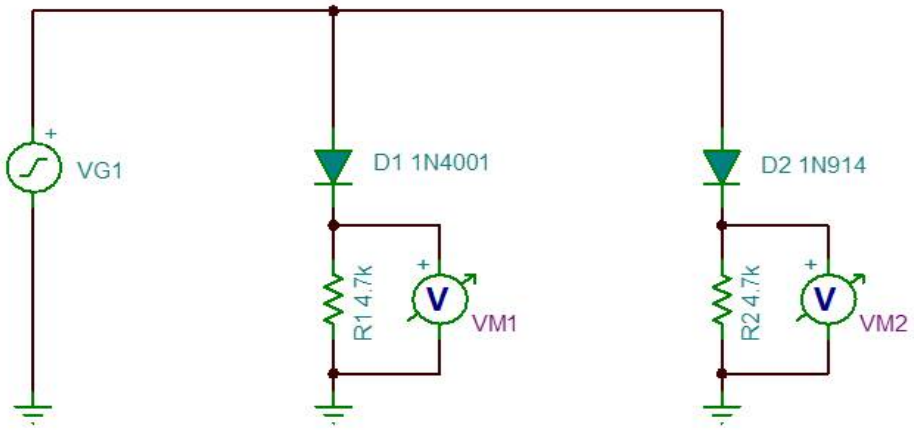

Figure 2.23: Comparison of fast recovery diode and slow recovery diode.

Another noise source present in the SMPS is rectifier diode noise. Shottky diodes are often used for the purpose of rectifying switched signal. In particular, in the secondary side of the transformer, a fast recovery type is used instead of a general schottky

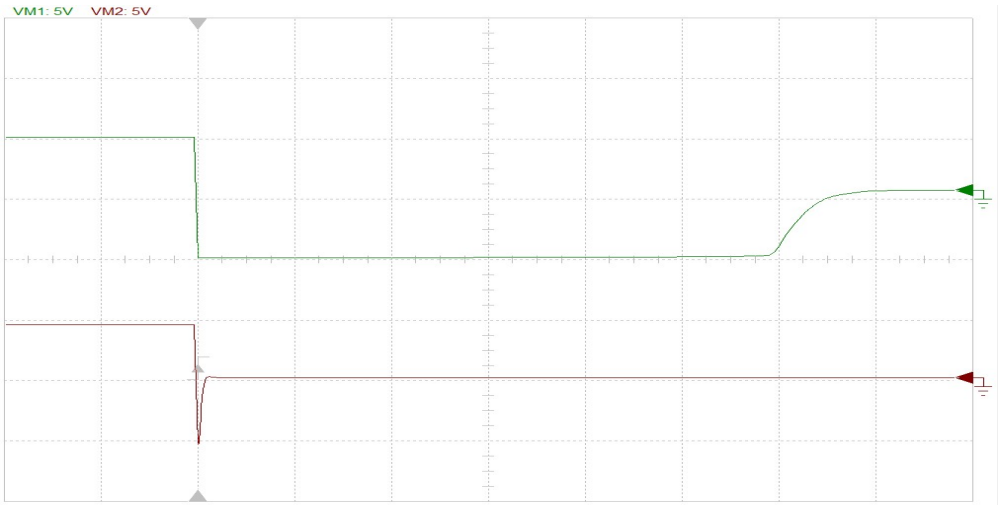

Figure 2.24: SPICE simulation result of recovery time.

diode. When a diode is forward-biased, charges are stored in the diode's capacitance. Conversely, when a diode is turned off, these charges disappear. This process is called diode recovery time, and difference between the diode with a fast recovery time and a diode with the slow recovery time is designed using the SPICE tool in Figure 2.23. Figure 2.24 shows the simulation result. It shows the recovery time after passing through the diode when a 5V square wave of 1kHz is applied to the input power. The recovery speed is faster than the general type, but a large ringing may occur in the timing of turning the diode on/off. In Figure 2.24, the fast recovery type diode's recovery time is approximately $40\,\mathrm{ns}$. On the contrary, the slow recovery type diode is approximately $3.5\,\mu\mathrm{s}$. It means, the fast recovery type diode has higher frequency spectra in the current than the slow type diode because of sharp edge. Moreover, the operating current on the secondary side is much larger than that on the primary side. As a result, rectifier diode noise has high-frequency and high-voltage, so it can be sufficiently operated as a major noise source.

Therefore, the SMPS manufacturers have to use a snubber circuit in parallel with the diode in the secondary rectifier circuit as shown in Figure 2.25. The snubber circuit

consists of an R-C series circuit and provides a current path through which charges stored in a capacitance of the diode are discharged when the diode is turned off. Typical values of them are approximately $470\,\mathrm{pF}$ and $10\,\Omega$. Also, LC low pass filter is added to the SMPS to prevent high-frequency ringing noise from going out to the output as shown in Figure 2.25.

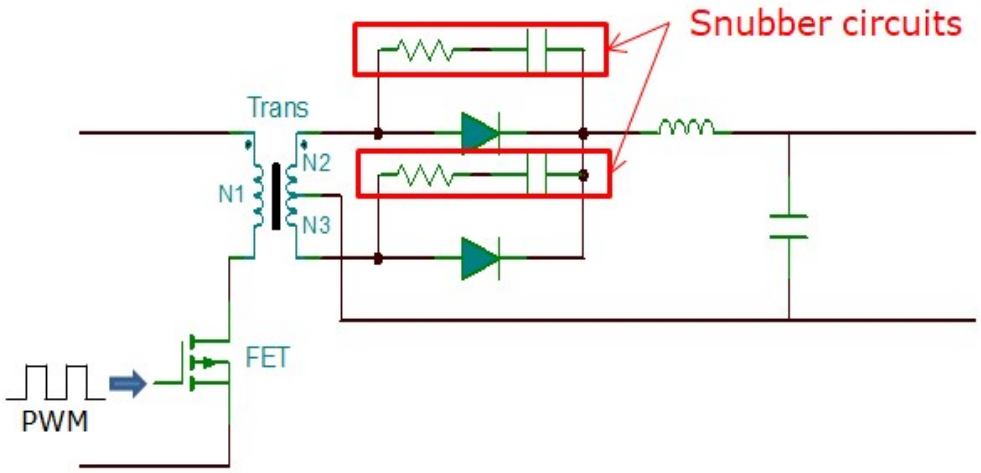

Figure 2.25: Snubber circuit of SMPS.

Chapter 3

ANALYSIS

The pulse generated in the HVG is rectangular shape and conditions of X-ray exposure are as follows.

- Tube voltage : $40\,\mathrm{kV}$(Anode $20\,\mathrm{kV}$ + Cathode $20\,\mathrm{kV}$).
- Tube current : $500\,\mathrm{mA}$.
- Exposure time : $100\,\mathrm{ms}$.

The tube voltage refers to the amplitude of the pulse voltage for X-ray exposure, and the value is the sum of $+20\,\mathrm{kV}$ and $-20\,\mathrm{kV}$ delivered to the anode line and cathode line in the tube. The tube current is the amount of current flowing from the HVG and exposure time is width of the pulse. The HVG rectangular pulse has rise time and fall time of approximately $1\,\mathrm{ms}$ regardless of the manufacturer. Ripple inevitably generated through the rectifier circuit is $1\%\sim4\%$ of kV, usually $800\,\mathrm{V}\sim1\,\mathrm{kV}$. However, this may differ depending on the manufacturer.

The DR HVG has some feedback points in the internal control board to check whether the X-ray pulse is well exposed. It is necessary to check whether it has an exactly rectangular shape and that there is no noise problem mentioned in Chapter 2. In Figure 3.1, the blue waveform is the X-ray pulse in the time domain and the yellow

is the FFT result. Amplitude and width of the pulse are as intended, but unintended high-frequency noise component is visible within the pulse width. The low-frequency of 100kHz can be observed as HVG ripple, but the noise approximately 10MHz is one of the problems mentioned in Chapter 2. Since it occurs only within the pulse width, it can be observed that it is not the effect of the reflected wave. Figure 3.2 shows spread waveform of Figure 3.1. Therefore, it can be expected that rectangular pulse itself does not acts as a noise source, but the high-frequency noise carried in the pulse would be a noise source and this is the shot noise.

It is necessary to define the source and parameters for the equivalent circuit analysis. First, The source is a 100KHz sine wave mixed with a 10MHz damped sine wave approximately 800V as shown in Figure 3.3. Parameters for analysis are as shown in Table 3.1. The coupling length of the high-voltage cable and the signal cable is $1\,\mathrm{m}$, and to clarify the role of the ground, the UL1005 6AWG earth cable is tied together. Each end of the Signal cable was terminated with $10\,\mathrm{k}\Omega$ resistance and measured coupling voltage at FE.

In the DR system, the high-voltage cable is much shorter than the wavelength ($15\,\mathrm{m}$) at the operating frequency (approximately $100\,\mathrm{kHz}$), and the braided-shield is much thinner than the skindepth ($0.12\,\mathrm{mm}$). Therefore, in this study, the relationship between the cables and ground plane can be analyzed in the form of a lumped circuit.

The capacitive coupling and the inductive coupling can be expressed as a mutual capacitance and a mutual inductance, respectively. The conductor that transmits the noise source is called the generator, and the conductor that is damaged is called the receptor. The total coupling voltage seen in the receptor is sum of the capacitive coupling and the inductive coupling [7].

$$V_{NE} = V_{NE}^{CAP} + V_{FE}^{IND}, \tag{3.1}$$

$$V_{FE} = V_{FE}^{CAP} + V_{FE}^{IND}. \tag{3.1a}$$

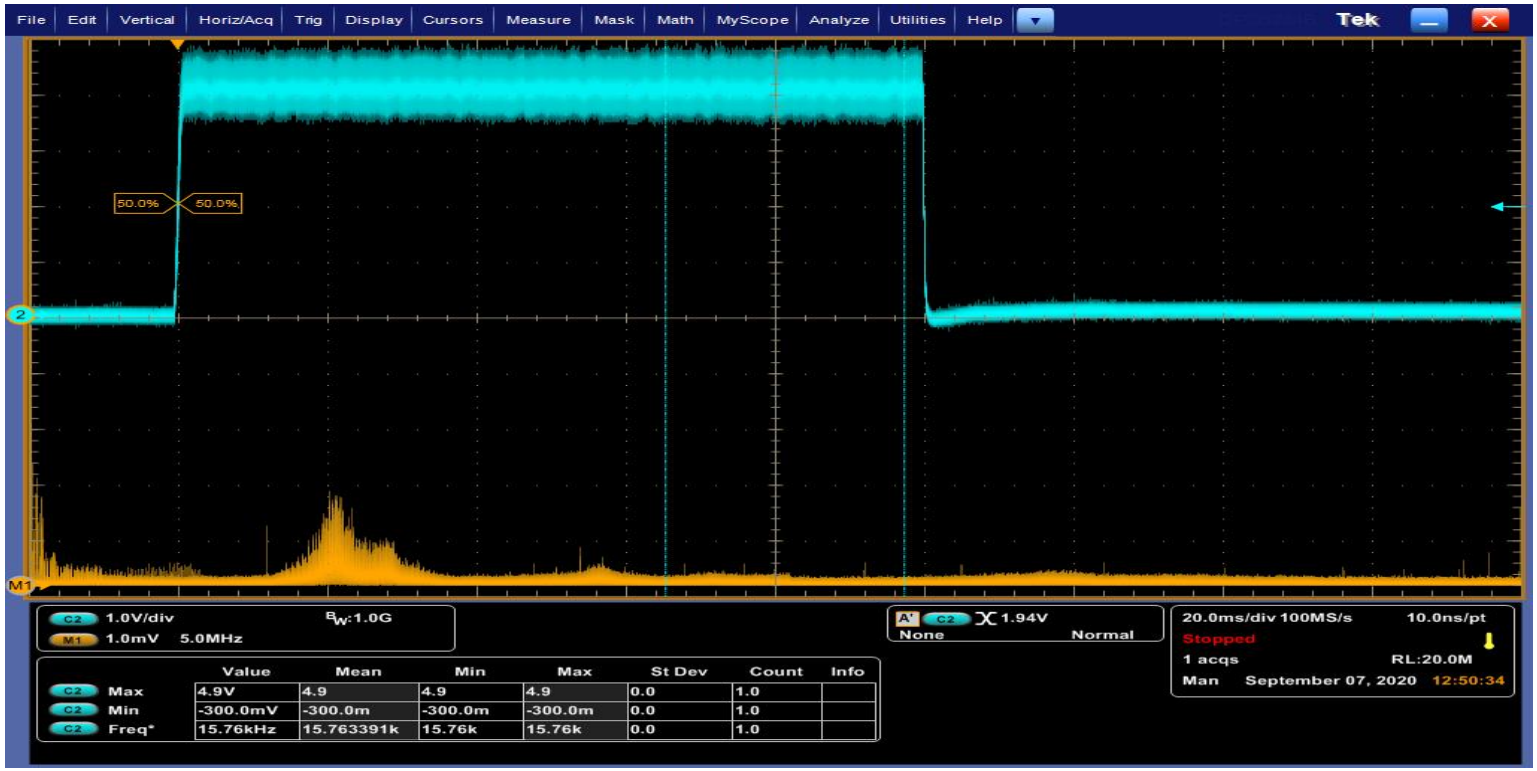

Figure 3.1: DR HVG output feedback waveform.

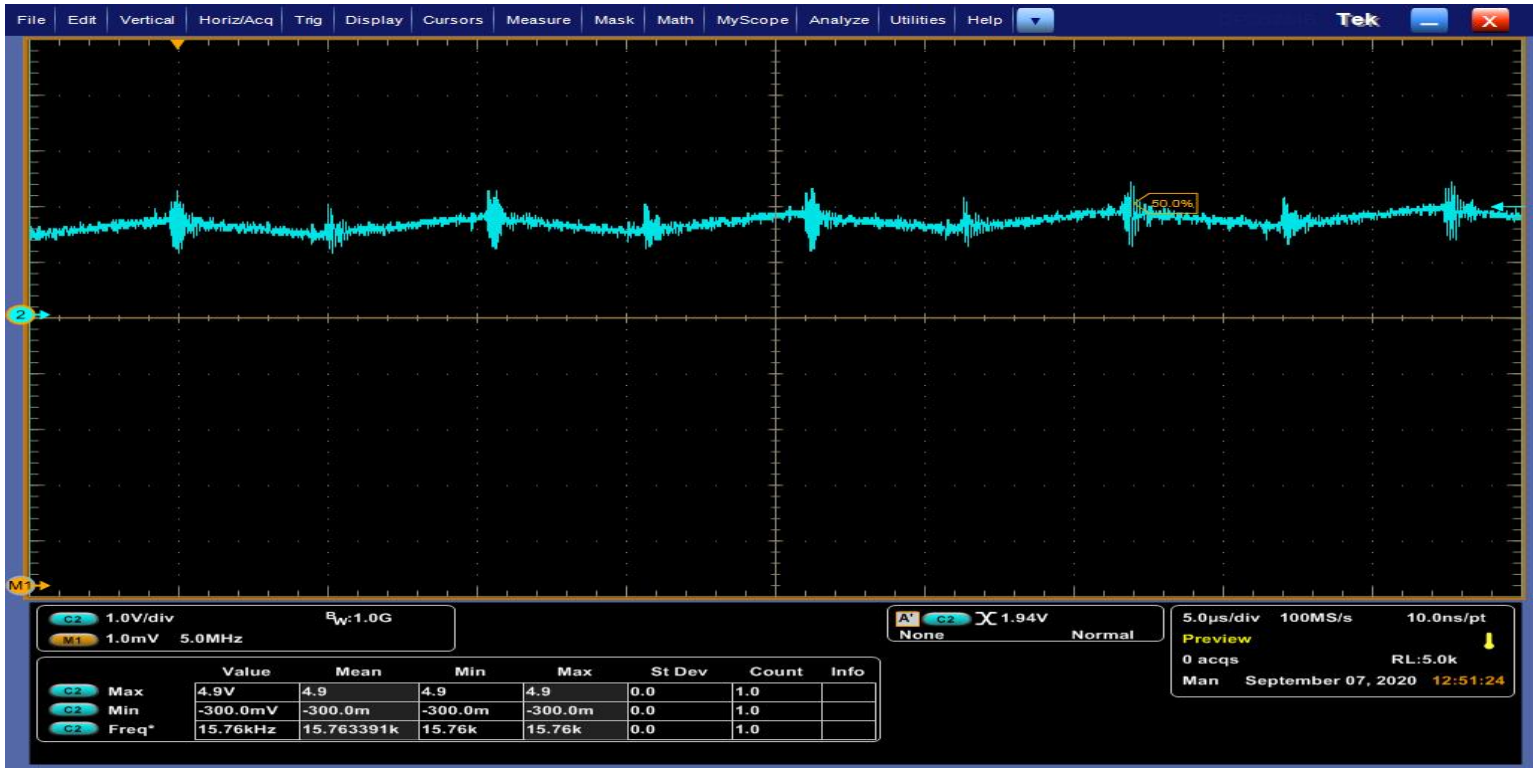

Figure 3.2: DR HVG output feedback spread waveform.

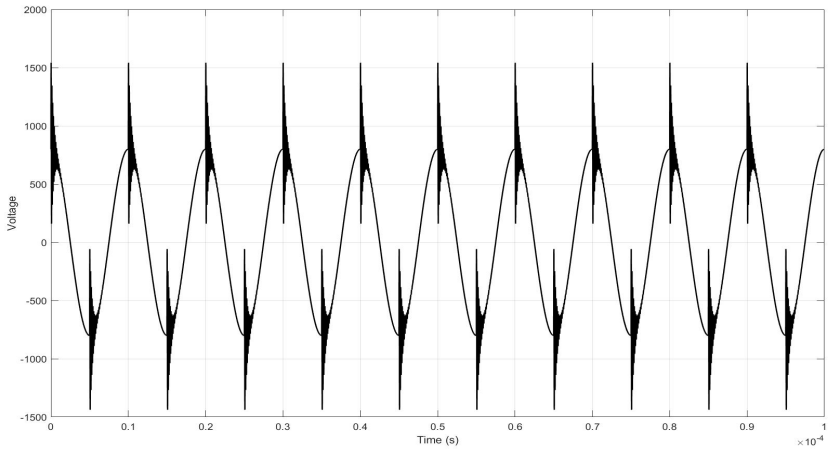

Figure 3.3: Source waveform.

Table 3.1: Setup parameters of DR case.

Parameter	Variable	Value	Units
Coupling Length	cl	1	m
Height above ground	h	0	m
Diameter of generator	dwg	1.98	mm
Diameter of receptor	dwg	2	mm
Diameter of the shield	$dwsg$	14.46	mm
Weave angle	$theta$	72	°
Separation	s	touching	-
Load impedance	Z_{FE}, Z_{NE}	10	kΩ
Number of Carrier	C	24	ea
Number of strand wires	N	12	ea
Principal axis length of aperture	L	0.6	mm

3.1 Equivalent Circuit of Capacitive Coupling

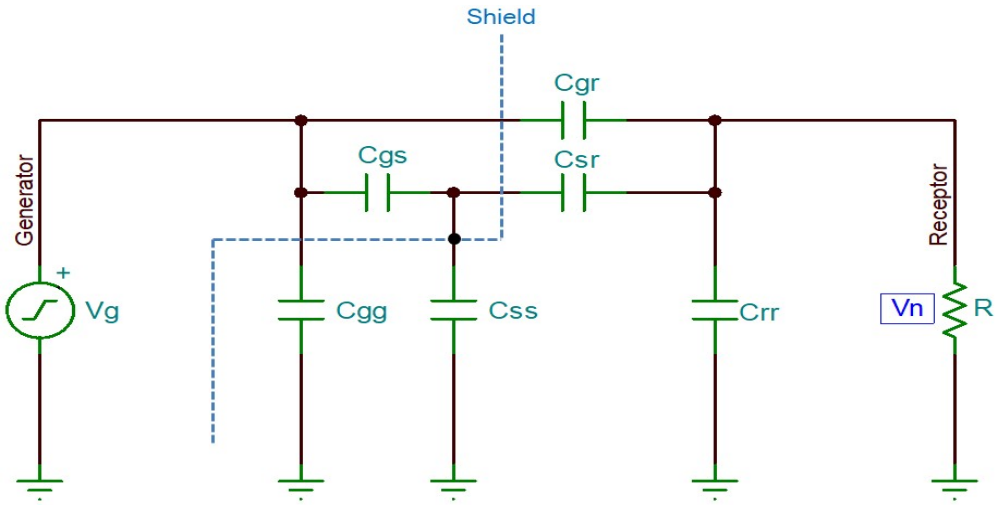

Figure 3.4: Equivalent circuit of the capacitive coupling of the DR system.

Figure 3.4 shows an equivalent circuit model of the DR capacitive coupling. Since both ends of the shield of the high-voltage cable are completely grounded 360°, the capacitance related to the shield can be neglected. The situation is the same as the well-grounded shield case in Chapter 2. Therefore, the formula is also same with Equation (2.14).

The capacitive couling result analyzed by the equivalent circuit is shown in Figure 3.5. Equation(2.14) is plotted with V_g, which has amplitude of $800\,\mathrm{V}$, frequency of $100\,\mathrm{kHz}$ sine wave mixed with $10\,\mathrm{MHz}$ damped sine wave. Coupling result is plotted in $+2.1 \sim -1.8\mathrm{V}$ of $10\,\mathrm{MHz}$ component and $\pm 0.1\,\mathrm{V}$ of the $100\,\mathrm{kHz}$ component.

3.2 Equivalent Circuit of Inductive Coupling

Figure 3.6 shows an equivalent circuit model considering only inductive coupling. Z_s and Z_l are the source impedance of HVG and the load impedance of the generator. However, it is difficult to express Z_s and Z_l equivalently due to the characteristics of

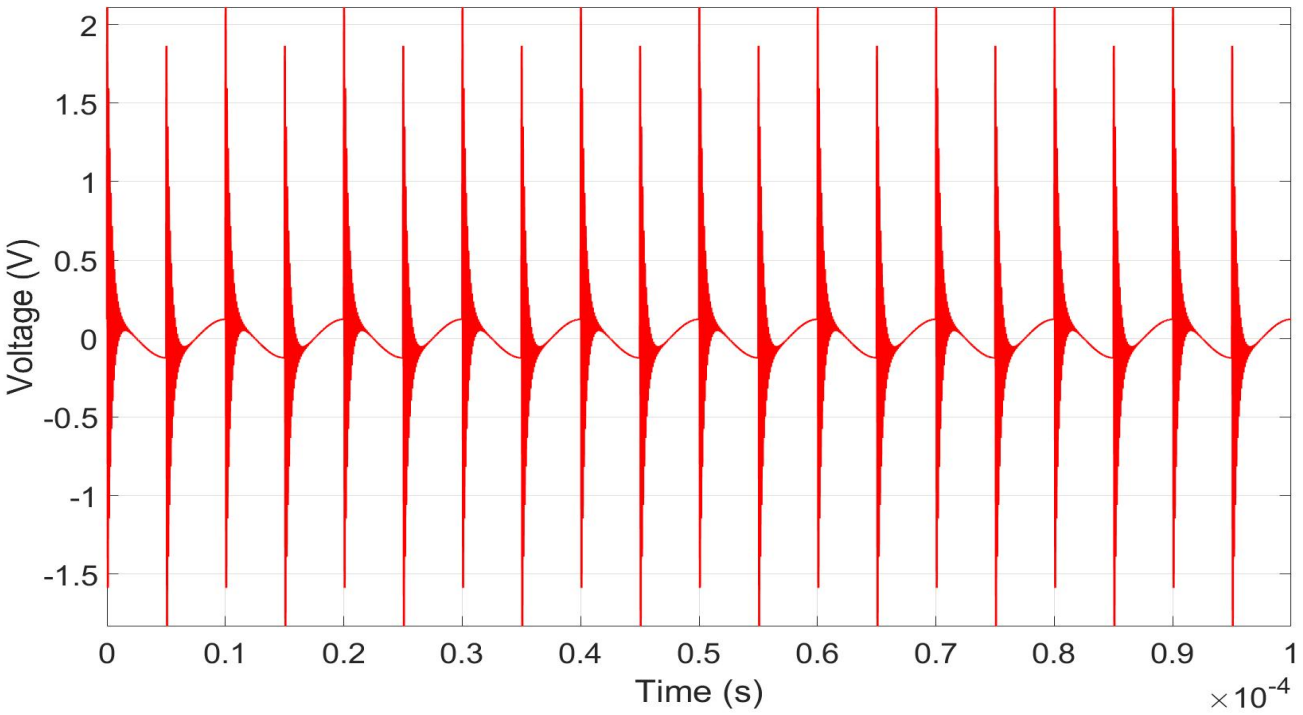

Figure 3.5: Capacitive coupling voltage at the receptor's far-end (FE).

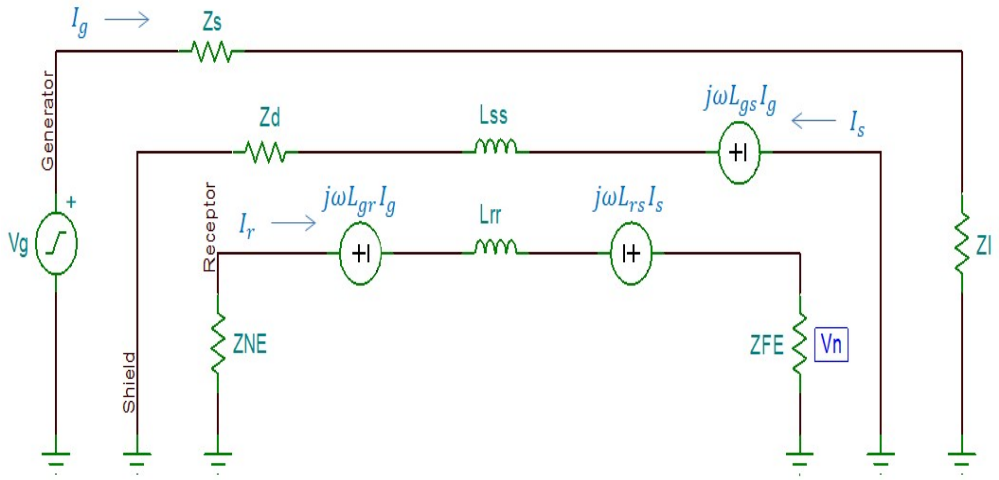

Figure 3.6: Equivalent circuit of the inductive coupling of the DR system.

the DR. In order to determine how much current (I_g) flows through the generator and whether the reflected wave does not occur, it is necessary to consider the characteristic impedance of the high-voltage cable along with Z_s and Z_l. However, we already know that I_g is $500\,\mathrm{mA}$, and DR products perform calibration work between the HVG and the tube in advance to completely transfer the power from HVG to the tube. If the calibration is well done, the reflected wave can be neglected in the equivalent model analysis because the intended power would have been well delivered to the tube. In other words, the setting values such as tube voltage, tube current, exposure time are same with the output waveform. If X-ray is shot without calibration, it will not be exposed with the intended conditions.

A resistance of shield Z_d and a mutual inductance between generator and receptor L_{gr} are expressed as the transfer impedance described above. Remaining L_{ss} and L_{rr} are the self inductance of shield and receptor, respectively. L_{gs} and L_{rs} are mutual inductance between shield and other conductors, respectively. Electromotive force is induced in the shield and receptor due to mutual inductance of L_{gr}, L_{gs}, L_{rs}, etc. As a result, the shield current I_s and the receptor current I_r are generated. When both ends

of the shield are completely grounded and the current is evenly distributed throughout the shield, the inductance of the conductor inside the generator and the shield is the same as the inductance of the shield itself ($L_{gs} = L_{ss}$). Similarly, a mutual inductance between the receptor and the shield L_{rs} is same as L_{gr} [7] [8]. The formula that summarizes V_{FE}^{IND} in terms of I_g is as follows.

$$V_N^{IND} = V_{NE}^{IND} = -V_{FE}^{IND} = I_g \times \frac{Z_{FE}(j\omega L_{gr} Z_d)}{(j\omega L_{ss})(Z_{NE} + Z_{FE} + j\omega L_{rr})}. \quad (3.2)$$

The result of the inductive coupling is approximately μV, so there is little effect. Because it is a voltage at FE, it shows a phase difference of 180° from the original signal as shown in Figure 3.7. As in Equation 3.1, the total coupling result is shown in Figure 3.8.

3.3 Equivalent Circuit of Shield Interruption

Predict the result in a situation where the high-voltage cable shield is partially broken and connects as pigtail. The DR HVG has very high-voltage, so if the shield is severely damaged, an immediate safety accident may occur. Therefore, validation through measurement is impossible and only the coupling level is predicted through the equivalent circuit analysis and simulation. As mentioned in Chapter 2, consider the length of the part where the interruption occurs in the total coupling length [6]. Coupling in the interrupted section is calculated as mutual coupling between two parallel wires. The formulas are as follows. L_{shield} is the length of shielded section, $L_{interrupt}$ is the length of interrupted section.

$$V^N = V_{shielded\,section} + V_{interrupted\,section}. \quad (3.3)$$

$$V_{FE}^{CAP} = V_g \times \frac{j\omega C_{gr} R}{1 + j\omega C_{rr} R + j\omega C_{gr} R} \times (L_{shield} + L_{interrupt}). \quad (3.4)$$

$$V_{FE}^{IND} = -I_g \times \frac{Z_{FE}(j\omega L_{gr} Z_d)}{(j\omega L_{ss})(Z_{NE} + Z_{FE} + j\omega L_{rr})} \times (L_{shield} + L_{interrupt}). \quad (3.5)$$

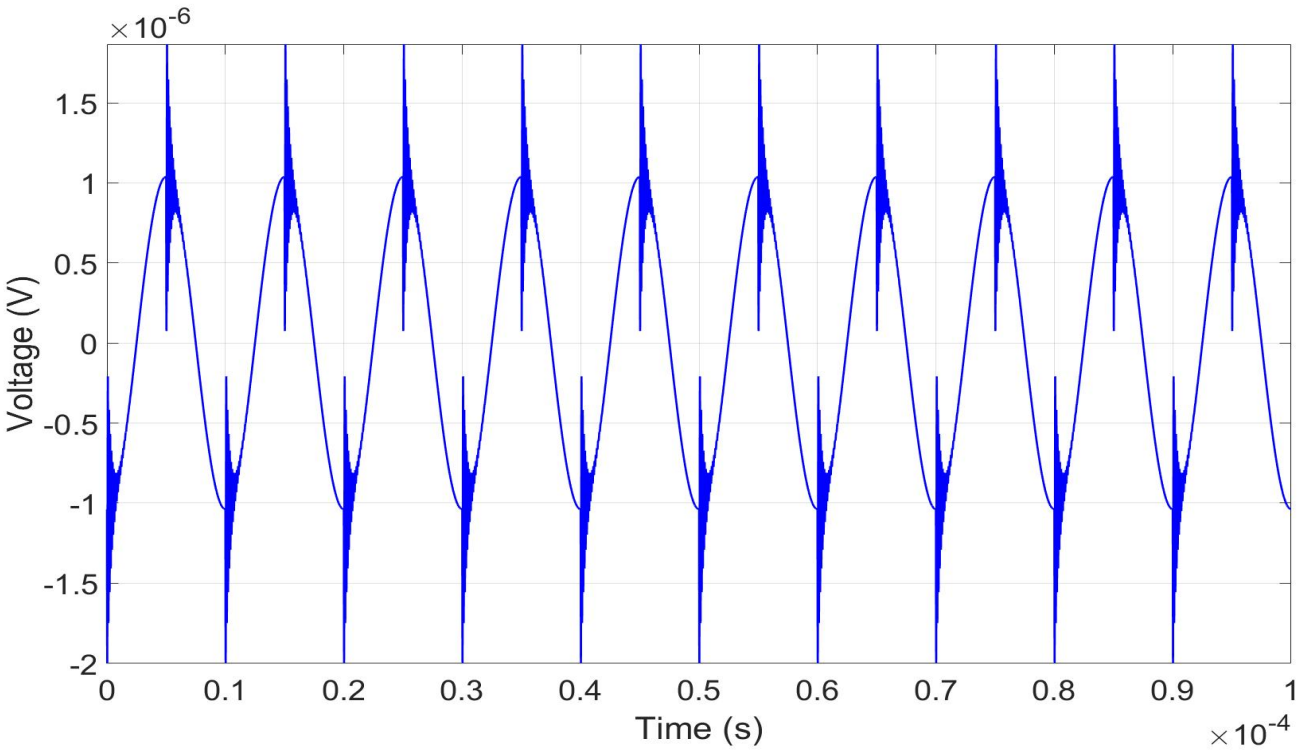

Figure 3.7: Inducitive coupling voltage at the receptor's FE.

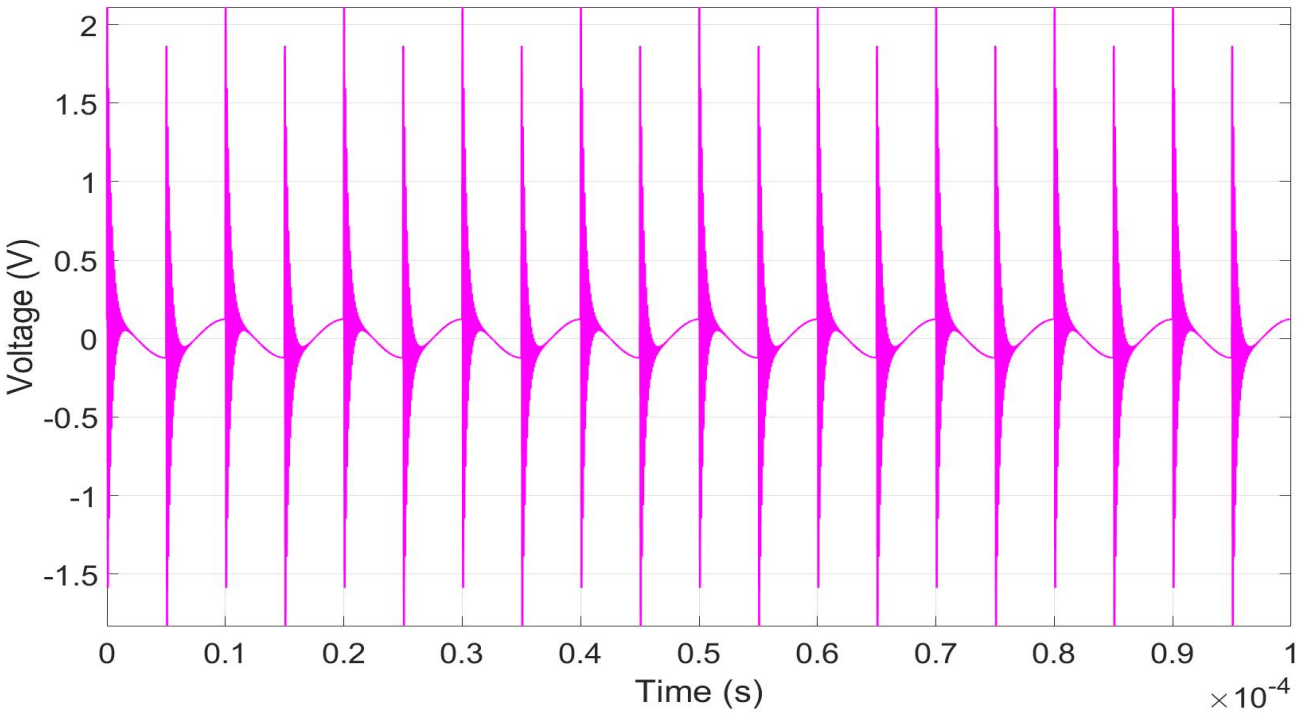

Figure 3.8: Total coupling voltage at the receptor's FE.

Since the cable is very thick, there will be no major damage to the shield even if there is severe friction or bending, so when only the aperture length is approximately 0.5cm and 1cm, the coupling voltage is shown as Figure 3.9 and 3.10. Voltage level is approximately 6.5V when the aperture length is $0.5\,\mathrm{cm}$. When the aperture length is $1\,\mathrm{cm}$, voltage level is approximately 12V. If there is no protection element, it may not only malfunction but also damage the control circuit.

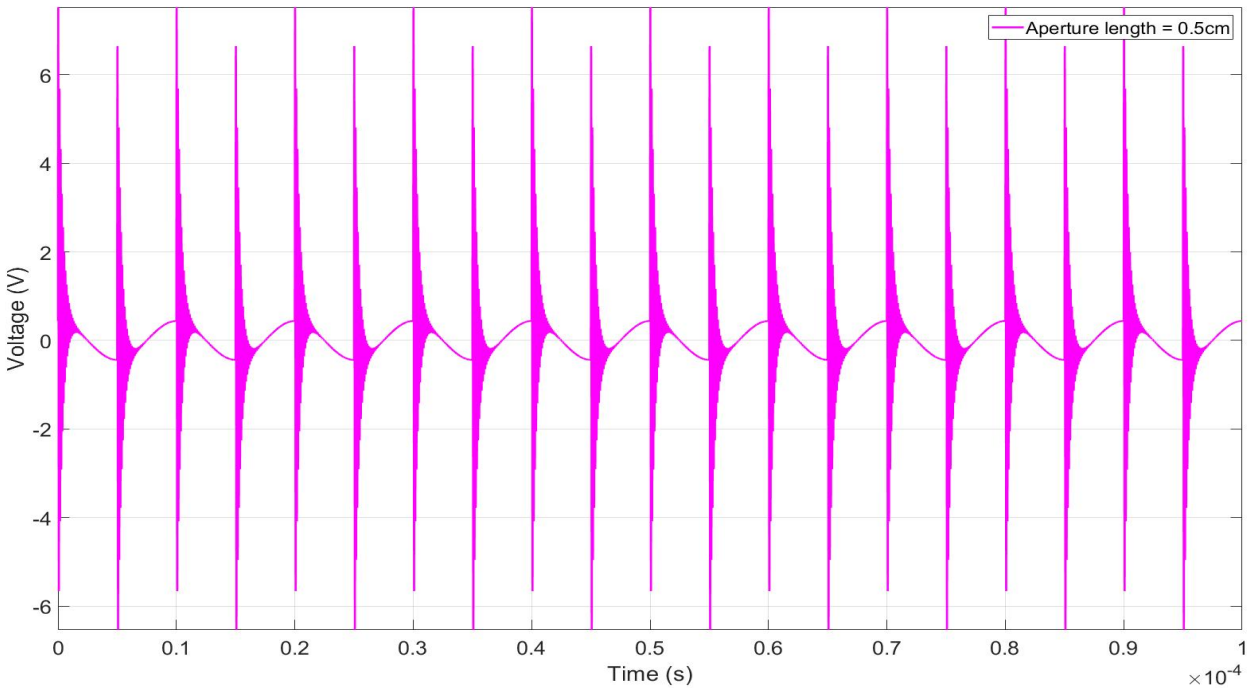

Figure 3.9: Total coupling voltage at the receptor's FE with the interrupted shield - 0.5cm.

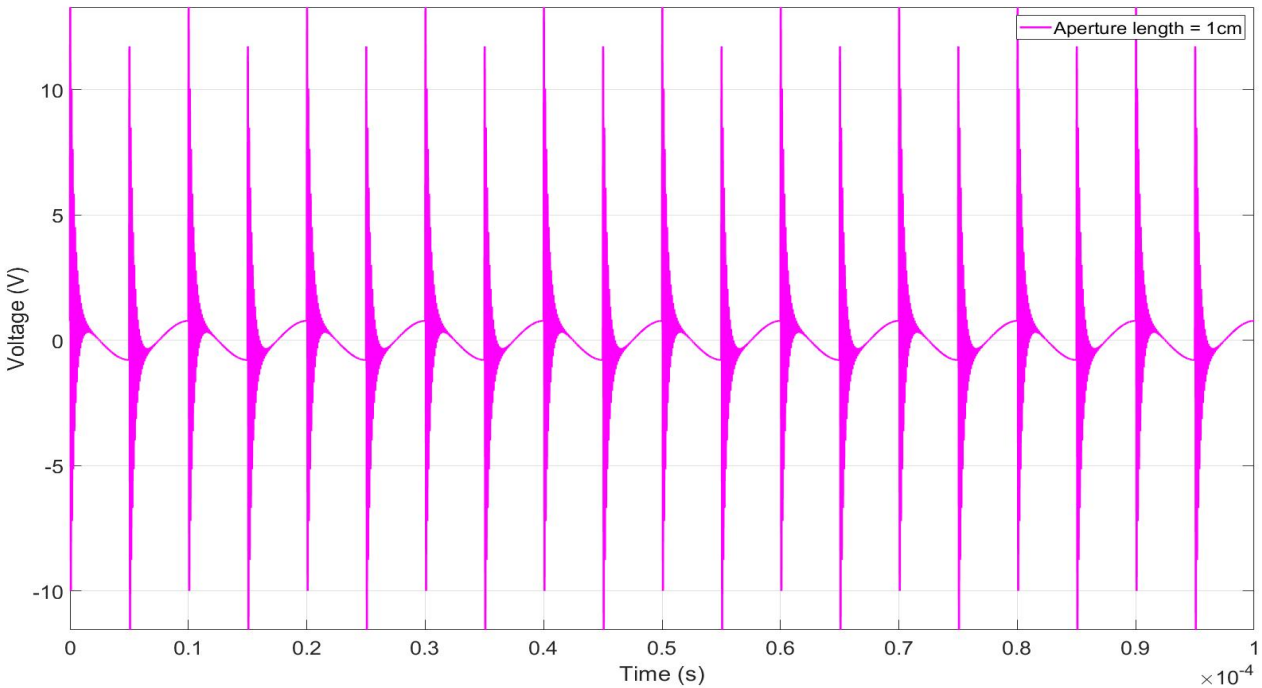

Figure 3.10: Total coupling voltage at the receptor's FE with the interrupted shield - 1cm.

Chapter 4

EVALUATION

4.1 Measurement

Validate through measurement the predicted coupling voltage using equivalent circuit analysis. The measurement environment is shown in Figure 4.1 and 4.2. Among the high-voltage lines from the HVG, the anode line is placed in a straight line, and the receptor line and the reference line is placed in a length of 1m on the same line. Measurements were made at the receptor FE, and the exposure conditions and cable specifications are consistent with those mentioned in Chapter 3.

4.1.1 Coupling Noise

Measurement result of the coupling is shown in Figure 4.3. In the left waveform of Figure 4.3, blue is the waveform of the HVG output voltage measured at kV feedback of the control board. Red is the measured voltage at the receptor FE. The waveform on the right shows the spread waveform of left. Yellow and green are a fast Fourier transform results for the kV feedback and the receptor FE. The coupling level observed at the receptor FE is approximately $2.4\,\mathrm{V}$. At this level of voltage can cause malfunction of the table or the stand. As mentioned earlier, the shape of X-ray pulse is rectangular pulse. However, as expected at Chapter 3, coupling waveform has high-

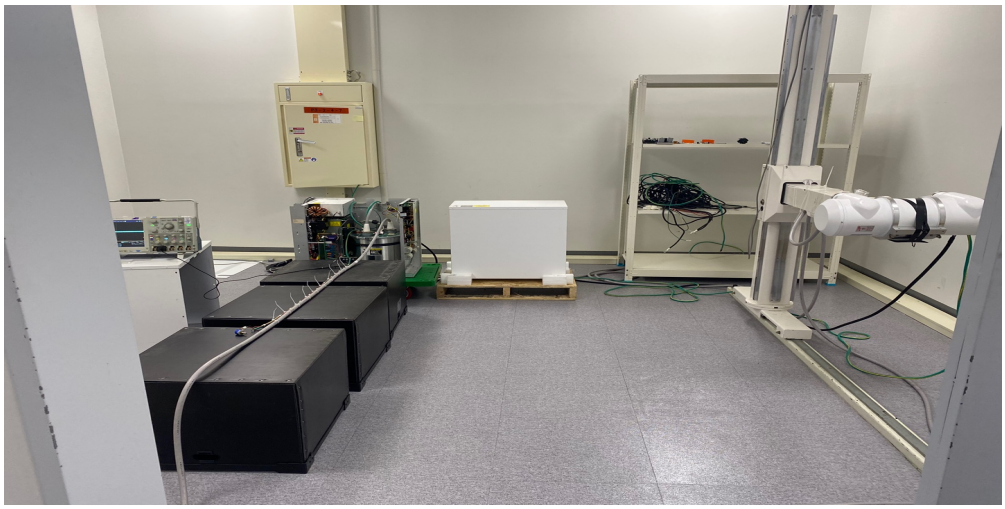

Figure 4.1: Measurement environment.

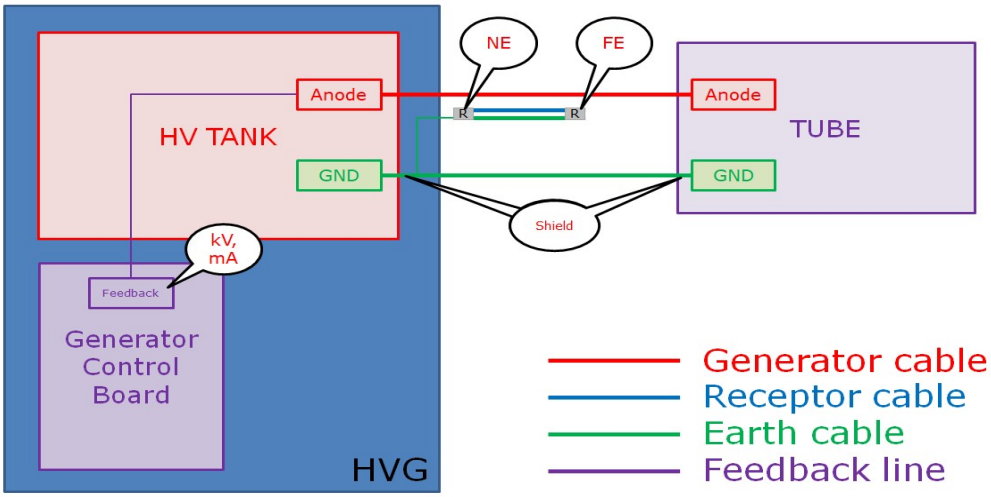

Figure 4.2: Block diagram.

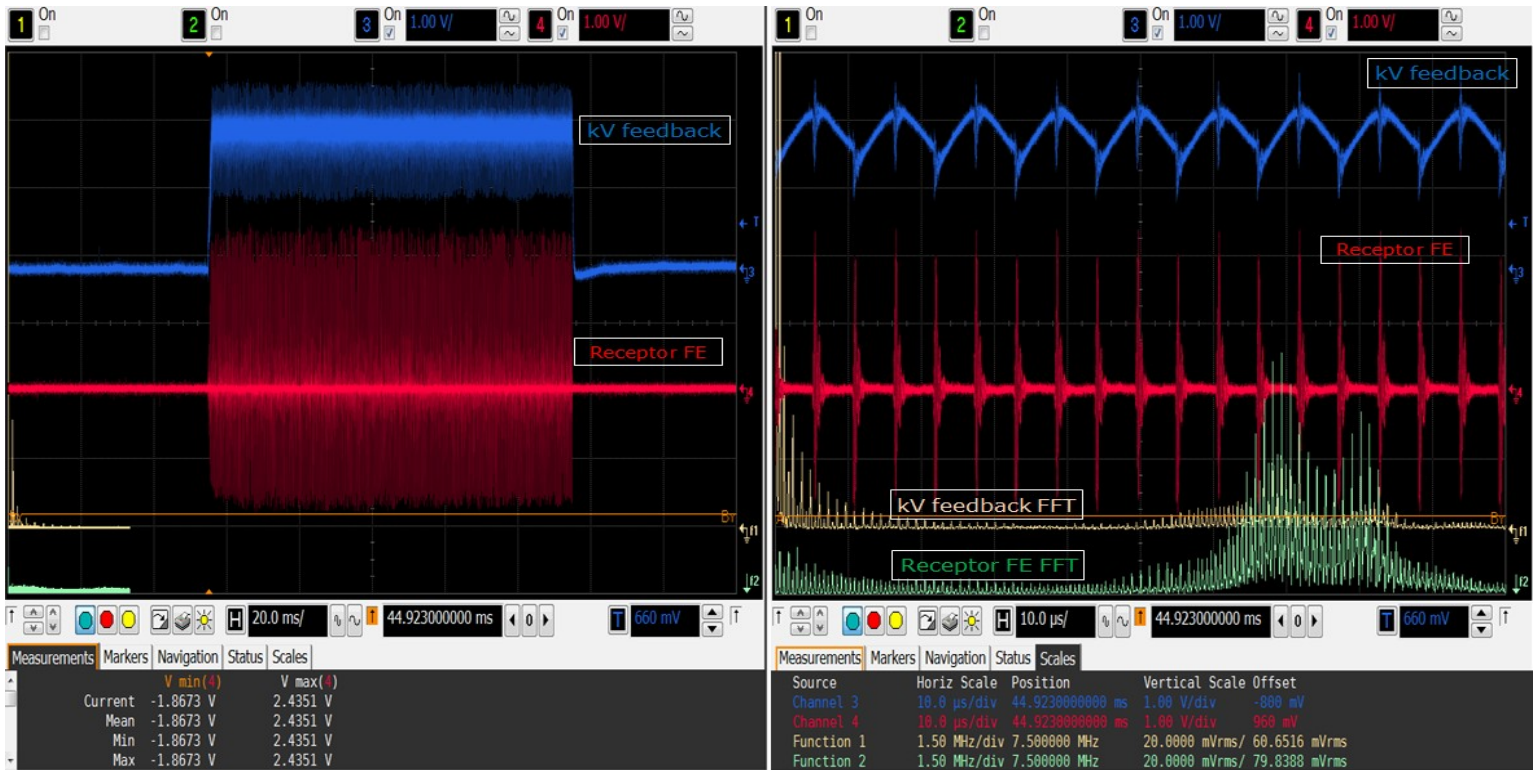

Figure 4.3: Measurement at the receptor's FE with a load impedance of $10\,\mathrm{k}\Omega$.

frequency noise. The low-frequency component, approximately 100 kHz seen in the FFT result is the ripple of the DR HVG, and this frequency is also described in the spec sheet. However, the high-frequency components approximately 10 MHz are not intended. When the rectangular pulse is coupled through the mutual capacitance, it is normal that the DC component disappears and only the spike component that may occur in the transient section is shown in Figure 2.5. However, 10 MHz noise is present throughout the pulse width and this is seen in the receptor FE.

Therefore, it is necessary to doubt the noises that can occur in the SMPS circuits discussed above. First, when the PWM inverter operates, ringing may occur at the on/off timing of the FET. As shown in Figure 4.4, if high-frequency ringing occurs in the PWM inverter circuit, it can be conducted to the HVG output through parasitic capacitance between the primary and secondary sides of the transformer.

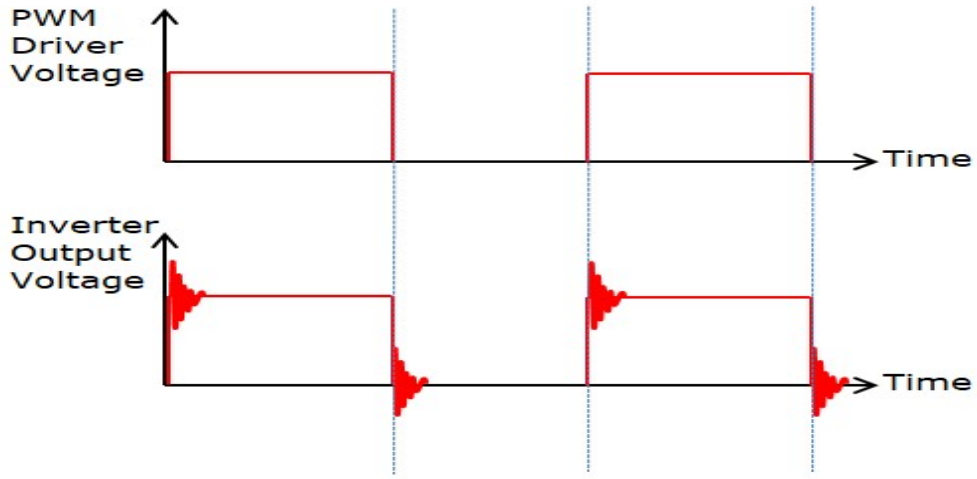

Figure 4.4: FET driver output ringing.

Figure 4.5 shows the current measured at the cable between the PWM inverter output and transformer input inside the HVG. Yellow is the inverter output waveform and green is the FFT result for inverter output. Unlike kV feedback, blue waveform, it operates only at 100 kHz cleanly. In addition, its shape is not rectangular as shown in

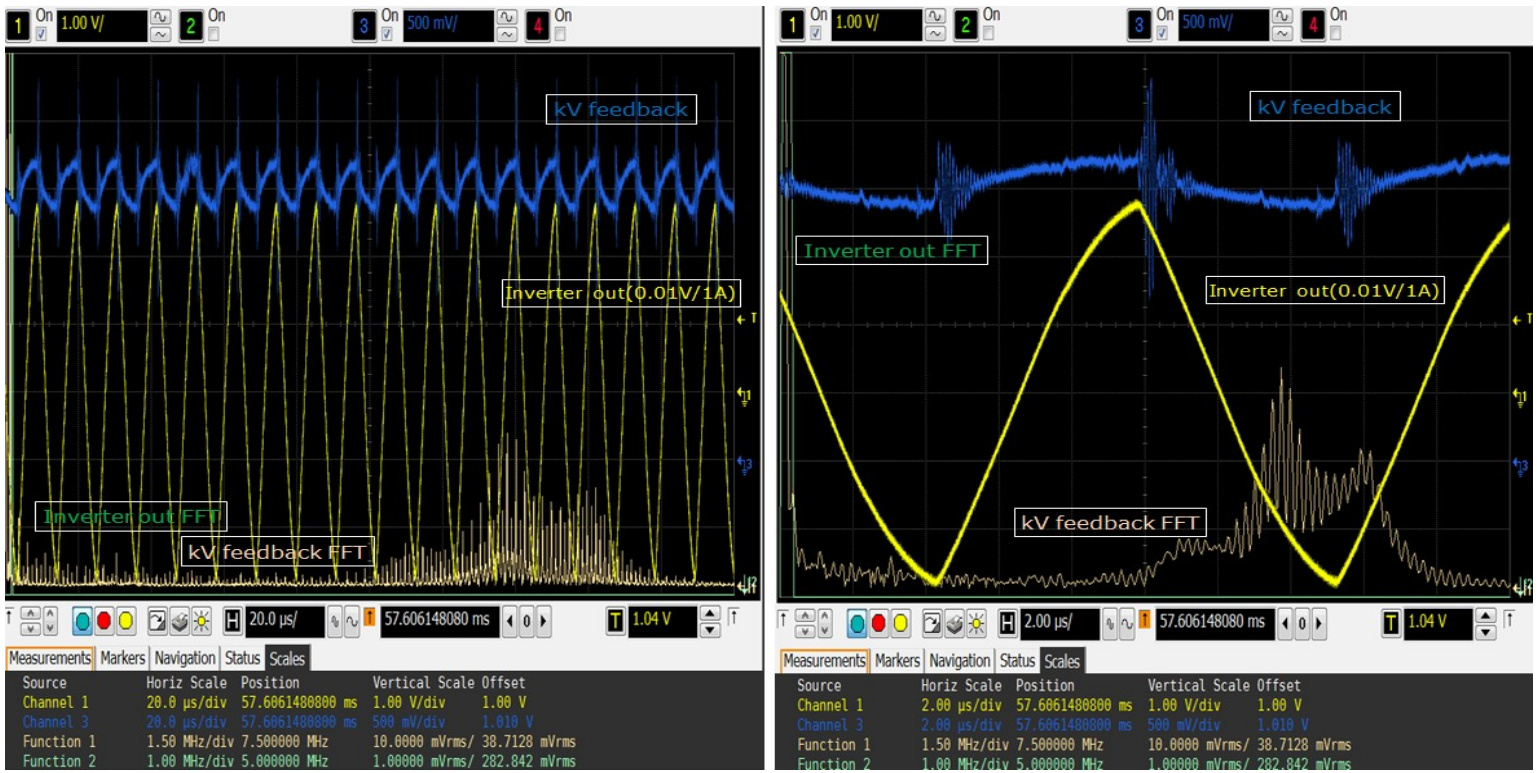

Figure 4.5: HVG PWM inverter output current.

Figure 4.4, but appears in a shape close to triangular. It seems that the transient section is reduced due to a large capacitance. In addition, the ferrite core was wound around the cable, so high-frequency noise could not pass through the transformer as shown in Figure 4.6.

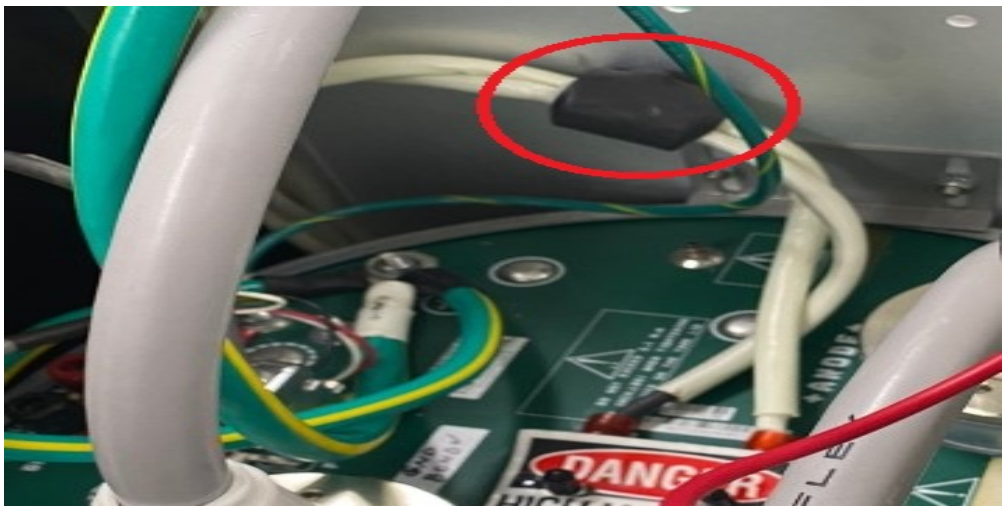

Figure 4.6: HVG PWM inverter output ferrite core.

Therefore, remaining possibility is the diode noise of the secondary side rectifier circuit. As already mentioned in Chapter 2, the diode of the rectifier circuit needs a snubber circuit in parallel, and additionally, there should be a low pass filter at the output stage. However, there was no snubber circuit in parallel with the diode and LPF at the output stage in the DR HVG, as shown in Figure 4.7. It's not just a specific HVG manufacturer's problem, and even if we checked the HVG of other manufacturer, there was no snubber circuit. Figure 4.8 shows receptor FE measurement result using other maker HVG. Like the previous measurement results, high-frequency noise appears as a coupling result and its level is similar.

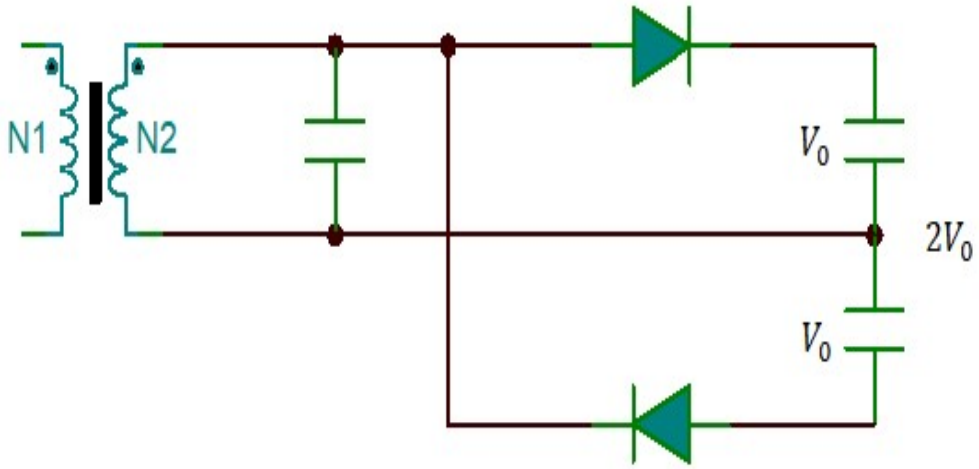

Figure 4.7: HV tank secondary voltage doubler.

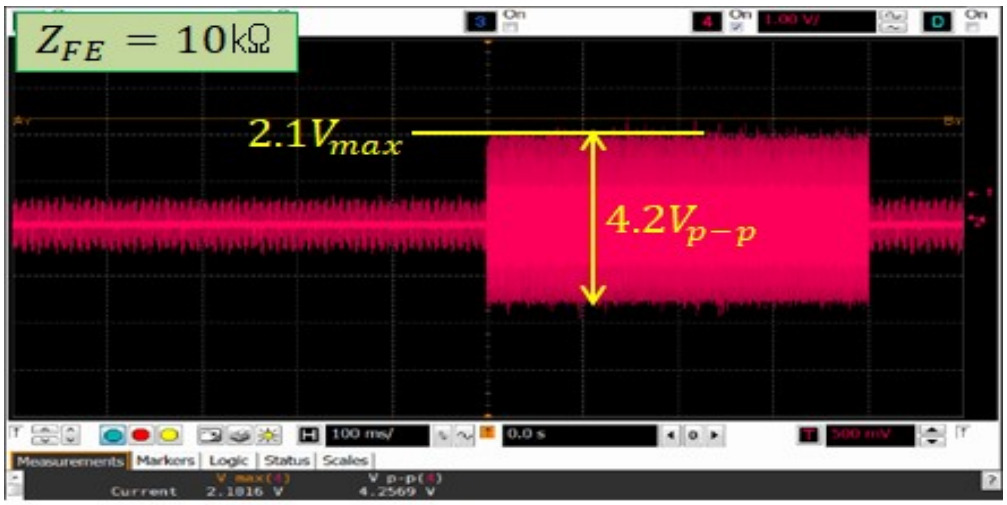

Figure 4.8: Measurement at receptor FE using other HVG manufacturer.

4.1.2 Solution

Now the components of the coupling noise seen in the receptor FE have been identified, EMC engineer has to do is find a noise reduction method. Most of all, since the voltage of the X-ray pulse is very high, the current is low, and the receptor NE and FE impedances are at the level of $10\,\mathrm{k}\Omega$, the coupling mechanism can be determined to be the capacitive coupling. Countermeasures for the capacitive coupling can be considered are as follows.

1. Shielding the receptor cable.
2. Increase the distance between the generator cable and the receptor cable.
3. Make the impedance of the receptor cable NE or FE close to zero.

Method 1 is the easiest way. However, as mentioned earlier, in the DR market where price competition is fierce, it is burdensome to change a general cable to a high-quality shielding cable. In addition, even if cable shielding is performed, if the shielding termination at both ends is not perfect, for example, in the form of a pigtail, the effectiveness of shielding is inevitably reduced. Method 2 can be a good option if you can change the cable path differently, but if you are a system engineer, you would know that it is impossible to fundamentally change the cable path. The remaining method 3 is the most effective and cost-saving method. Because it is impossible to remove the load attached to the receptor, a decoupling capacitor can be used to make the impedance appear close to zero only for high-frequency noise. Since R_{FE} and R_{NE} are equally $10\,\mathrm{k}\Omega$, a capacitor is added at FE to have much smaller impedance than the composite resistance $5\,\mathrm{k}\Omega$ at $10\,\mathrm{MHz}$ as shown in Figure 4.9.

From Figure 4.10 to 4.12 show results of decoupling capacitor method. When $10\,\mathrm{nF}$ is added to the FE as shown in Figure 4.10. Result of $100\,\mathrm{nF}$ is shown in Figure 4.11. Figure 4.12 shows result of $1\,\mu\mathrm{F}$ added. It can be observed that the coupling level has decreased to the range of -300 to $470\,\mathrm{mV}$. To find out why the coupling level does

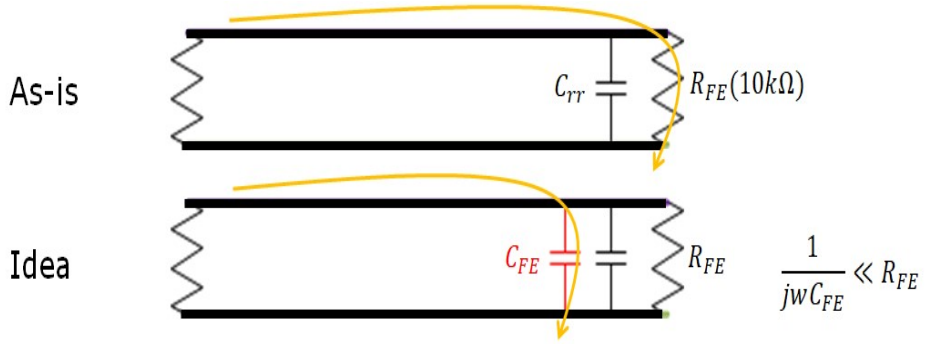

Figure 4.9: Receptor's FE with a decoupling capacitor.

not go down to 0 and maintains -300 to $470\ \mathrm{mV}$, the distance between the generator and the receptor is completely separated and measured. Result is shown as Figure 4.13. However, the result also remains at the range of -300 to $380\ \mathrm{mV}$. It means that -300 to $380\ \mathrm{mV}$ of noise is not caused by coupling, but a result of conduction by an oscilloscope.

Finally, we checked whether the solution used decoupling capacitor and the solution used additional shielding are on the same level. The measurement result after additional shielding on the receptor is -330 to $350\ \mathrm{mV}$ as shown in Figure 4.14. It is same as when the distance is completely separated. Considering the measurement error, it can be observed that there is no significant difference between the solution through capacitor and the solution method through shielding.

4.2 Simulation

Additional validation for measurement and analysis has performed using 3D simulator CST. First, cable modeling is shown in Figure 4.15. The generator cable and the receptor cable are closely adhered to each other with a length of 1m, and the 6AWG cable serving as the ground is laid in the same path. Since the effect of the ground plane cannot be completely ignored, it is modeled as being several meters away from

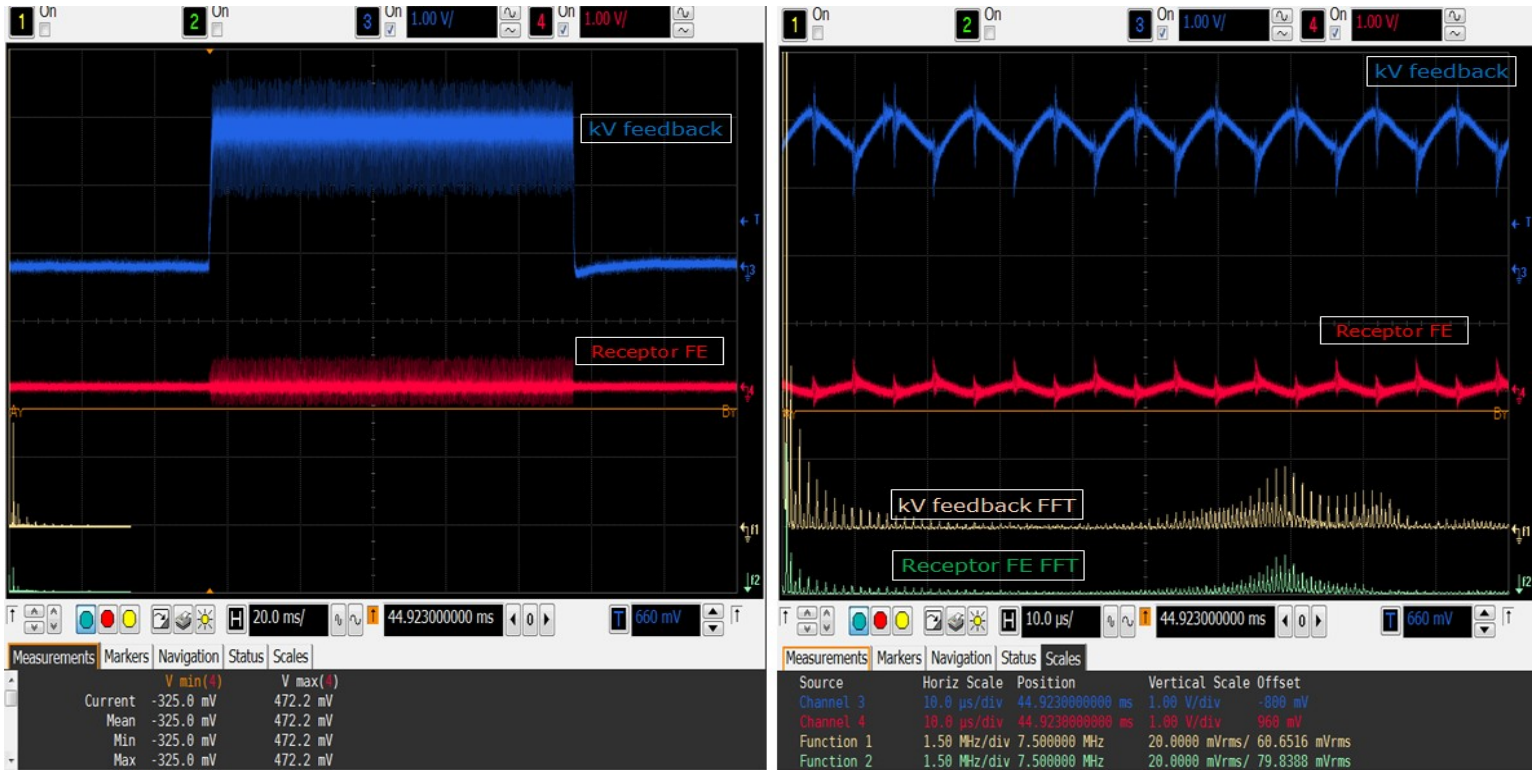

Figure 4.10: Measurement at the receptor's FE with a decoupling capacitor of 10 nF.

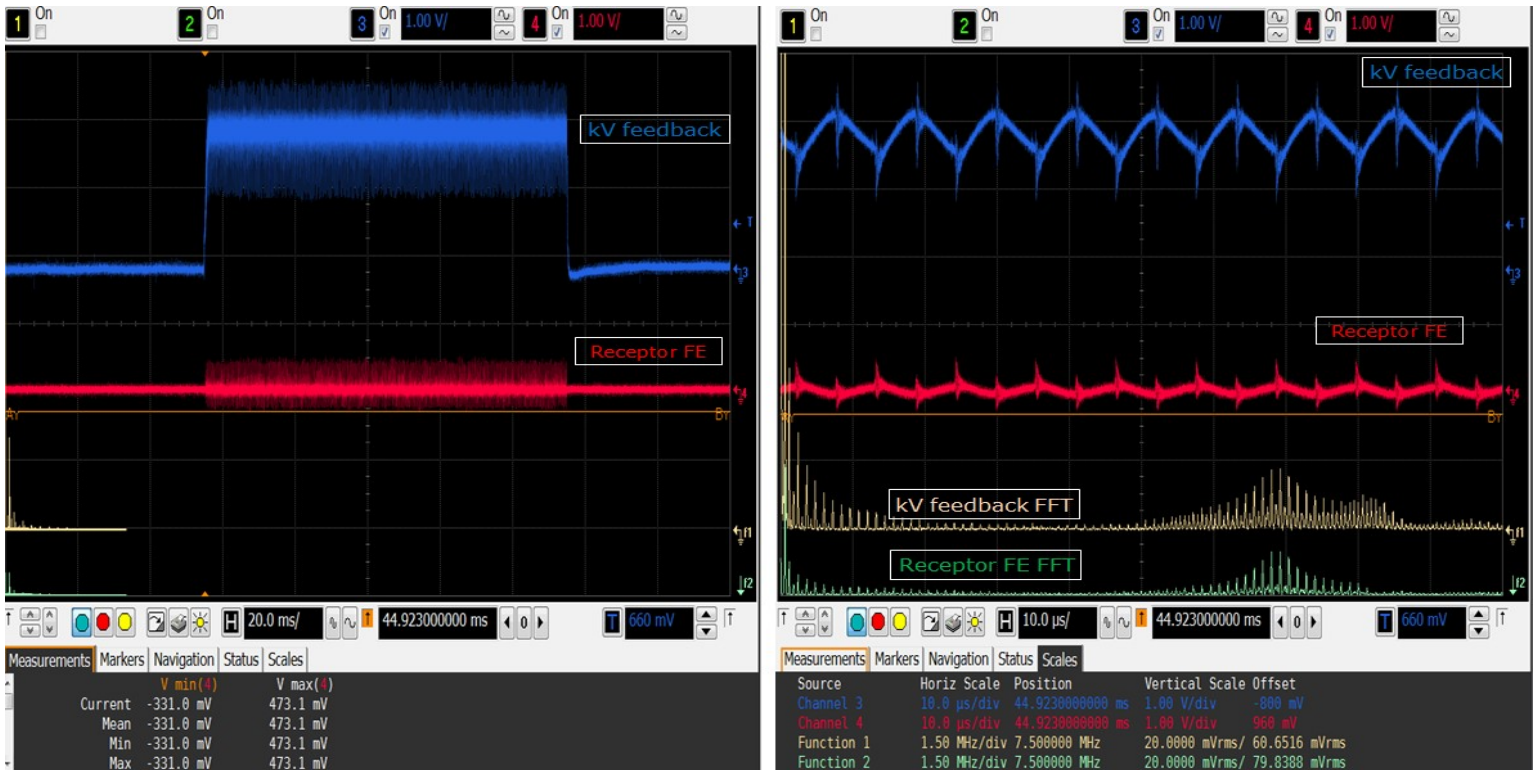

Figure 4.11: Measurement at the receptor's FE with a decoupling capacitor of $100\,\mathrm{nF}$.

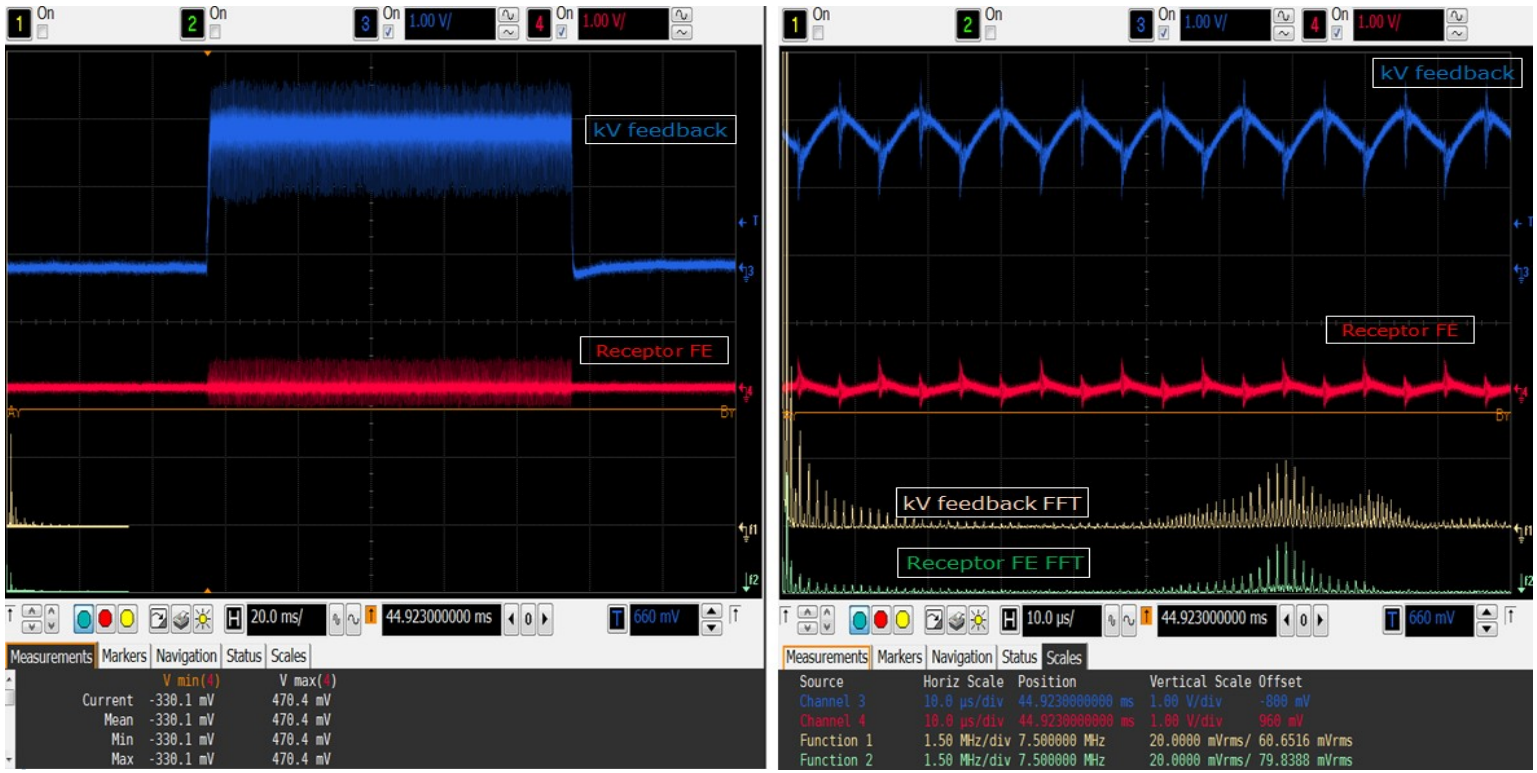

Figure 4.12: Measurement at the receptor's FE with a decoupling capacitor of 1 µF).

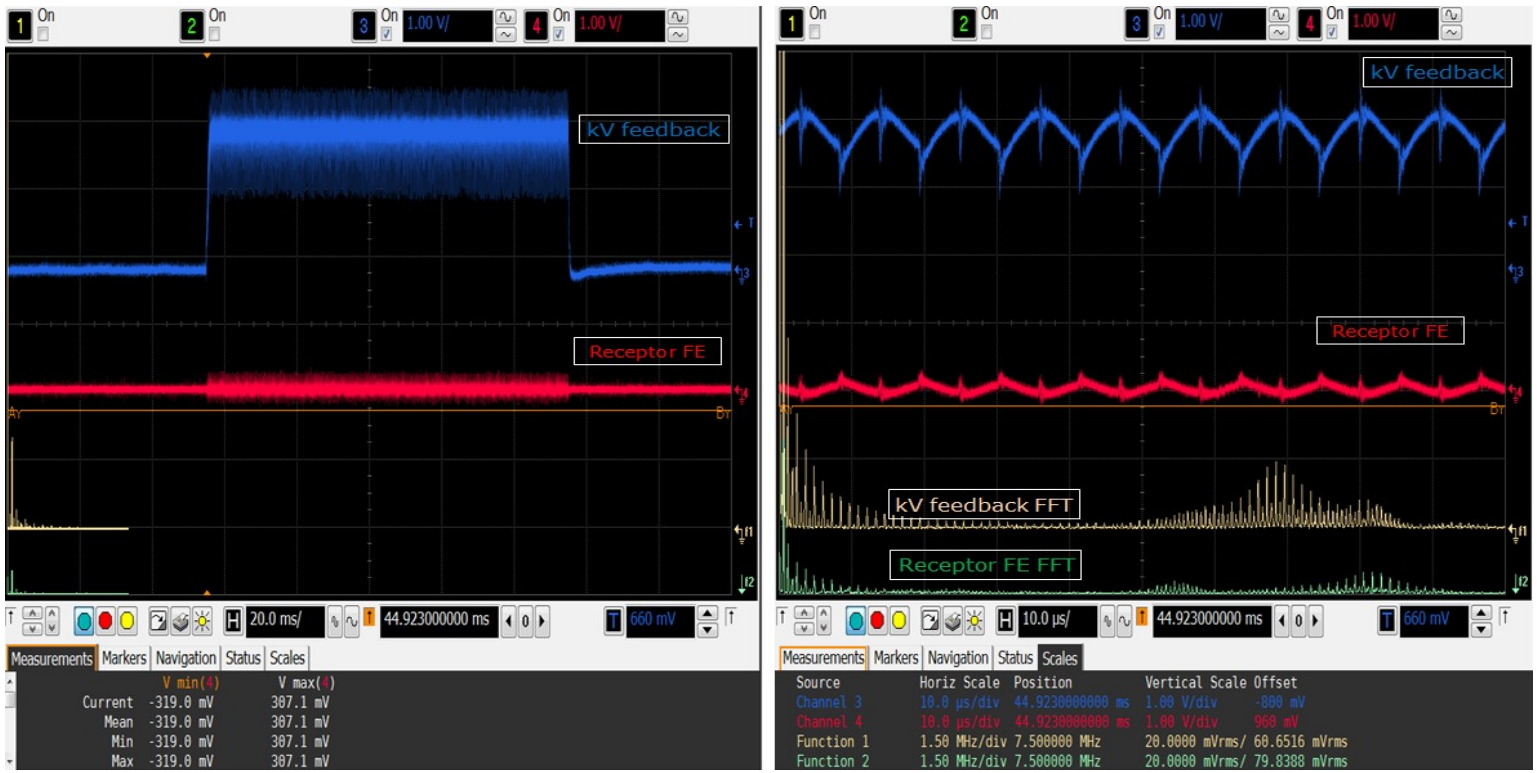

Figure 4.13: Measurement at the receptor's FE after the separation of cables

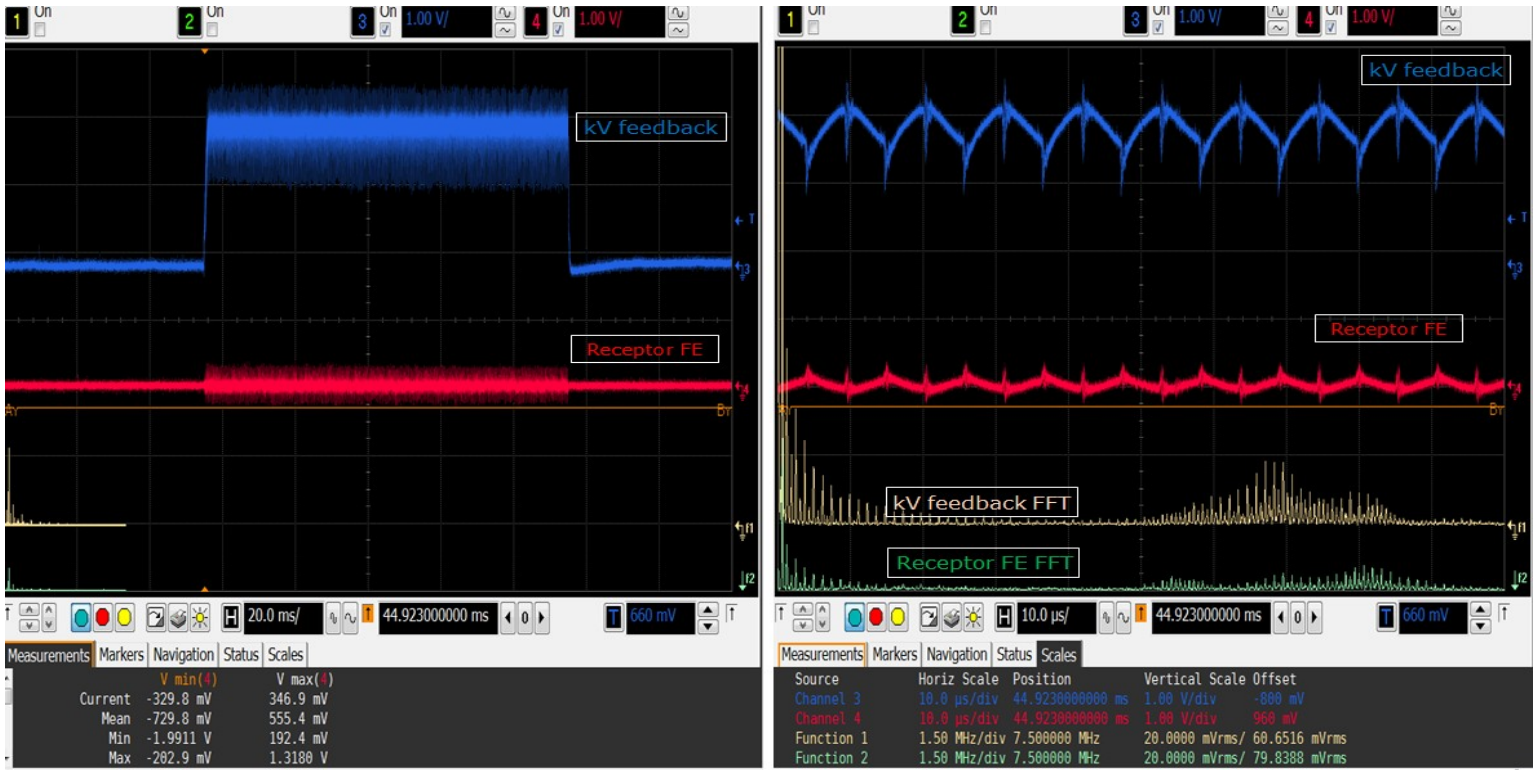

Figure 4.14: Measurement at the receptor's FE in the case where an additional shield is used.

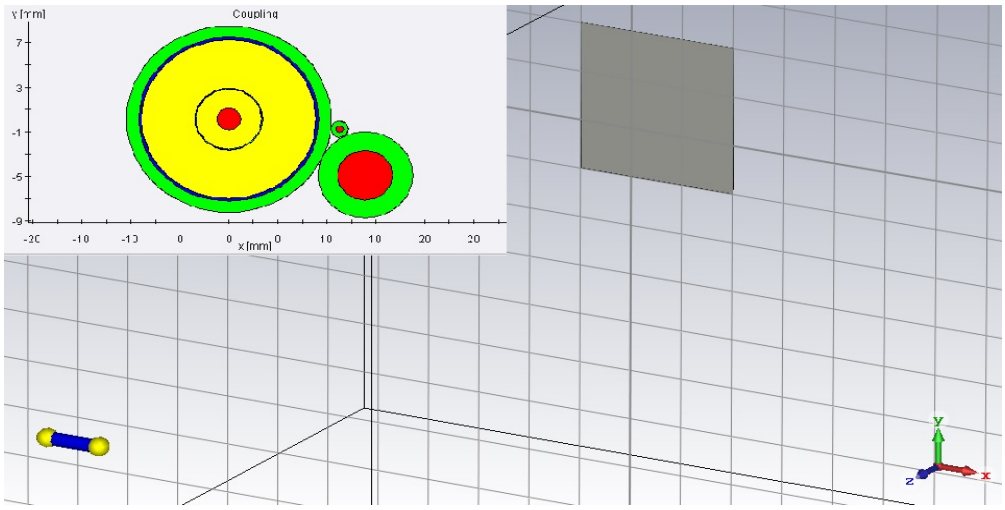

Figure 4.15: CST cable modeling.

the cable. The result of simulation by applying a noise source to the modeled cable and attaching lumped elements is shown in Figure 4.16. Similar to measurement and equivalent model, a $10\,\mathrm{MHz}$ component appears at the level of $+1.8 \sim -2.1\mathrm{V}$ with a period of $5\,\mu\mathrm{s}$ as shown in Figure 4.17. The difference from the measurement result can be explained by the difference in conduction noise that may occur during the actual measurement. In addition, in the case of the equivalent model, since the result is perfectly ideal, the level may be rather high because the impedance of the conductor itself or the parasitic component of the lumped element are not considered.

Effect of interrupted shield is modeled as shown in Figure 4.18. Figure 4.19 and 4.20 show simulation results according to variation of aperture length. Voltage level is approximately 6.5V when the aperture length is $0.5\,\mathrm{cm}$. When the aperture length is $1\,\mathrm{cm}$, voltage level is approximately 12V. Although the actual measurement was not possible due to safety issue, it is consistent with the result of equivalent circuit analysis using Matlab.

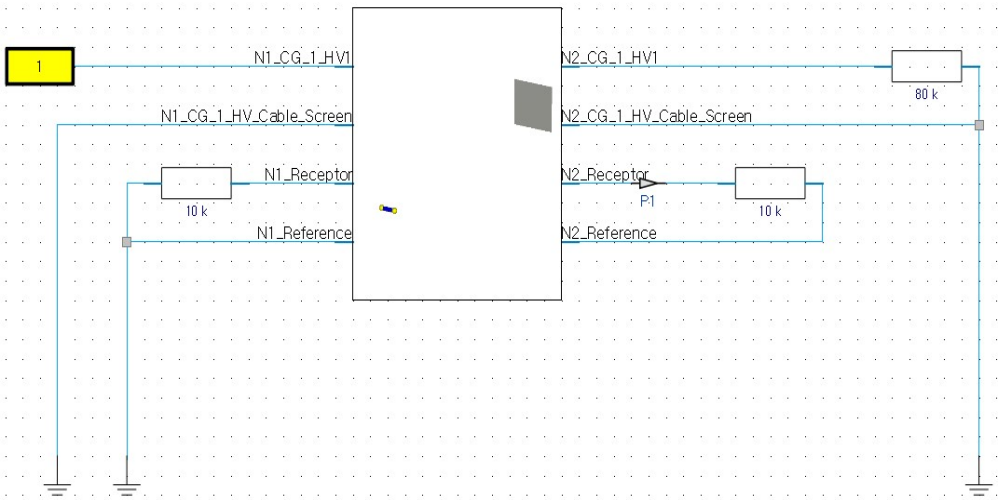

Figure 4.16: CST equivalent circuit.

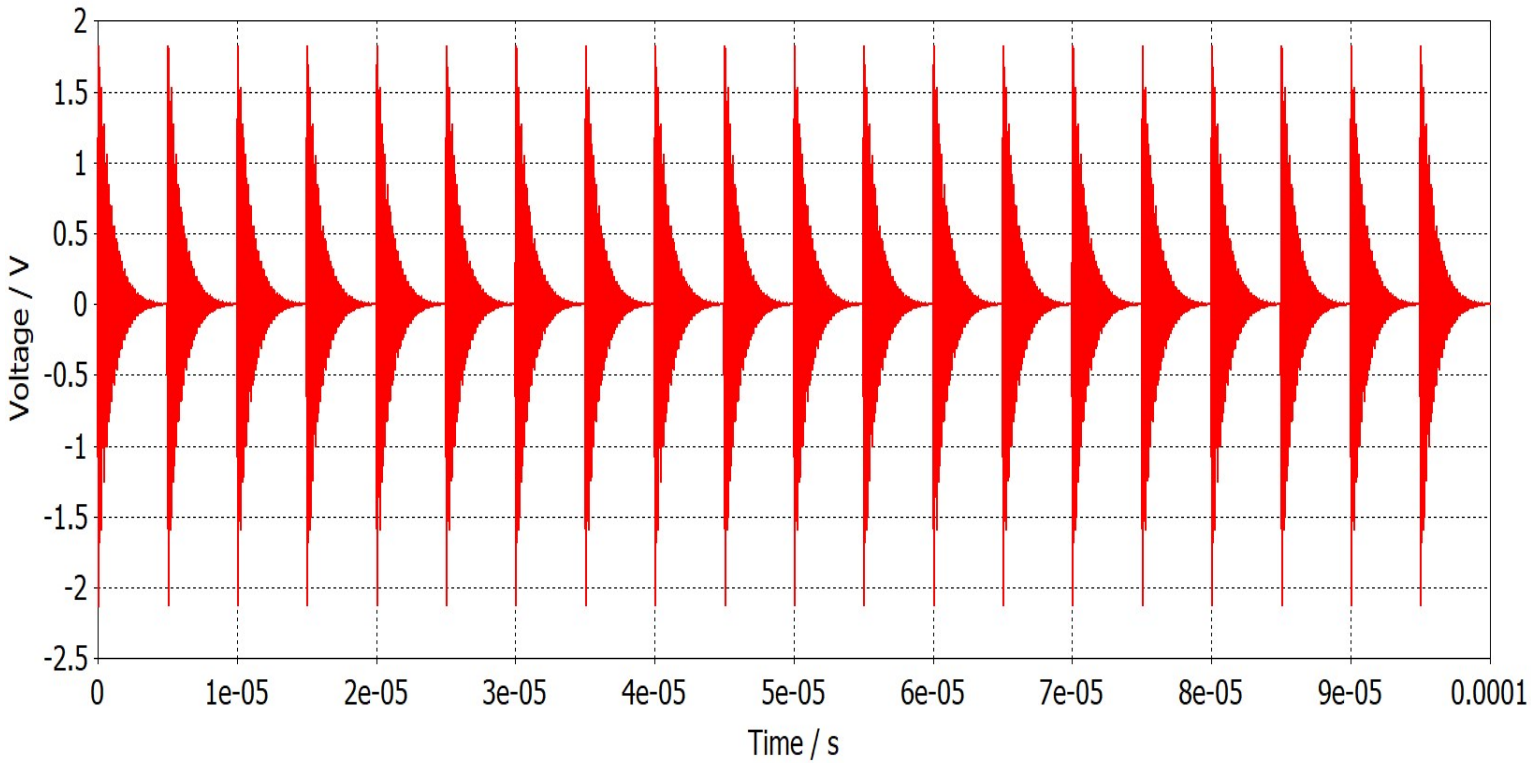

Figure 4.17: CST Simulation.

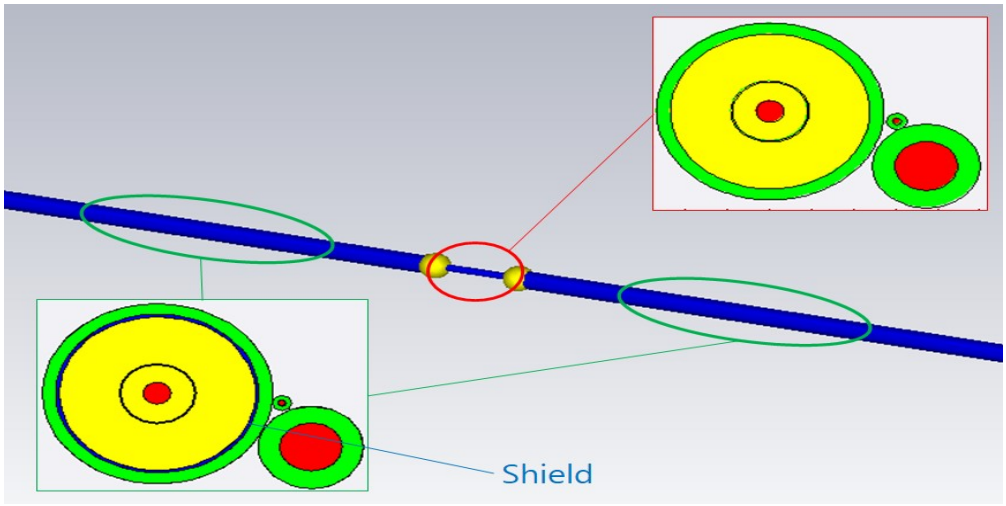

Figure 4.18: CST cable modeling with the interrupted shield

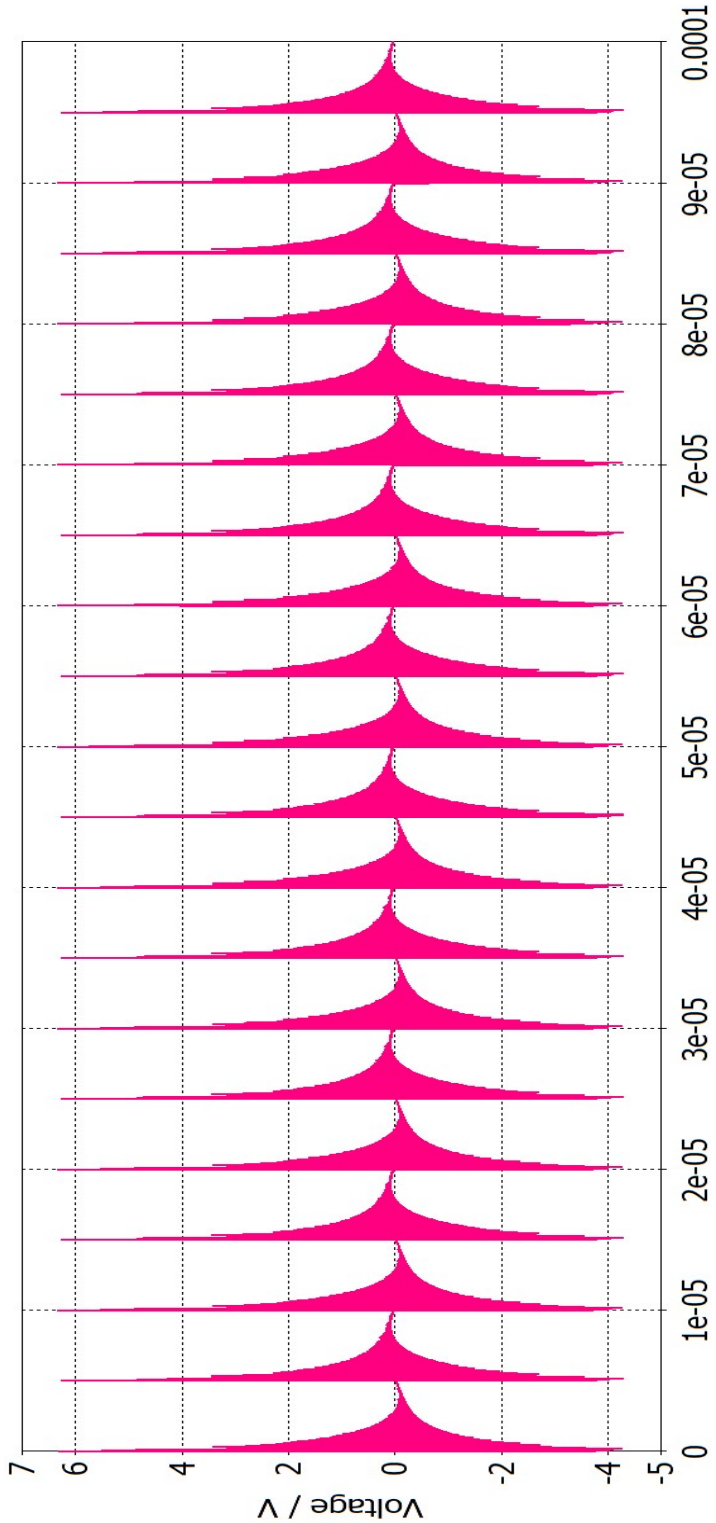

Figure 4.19: CST simulation with the interrupted shield - 0.5cm.

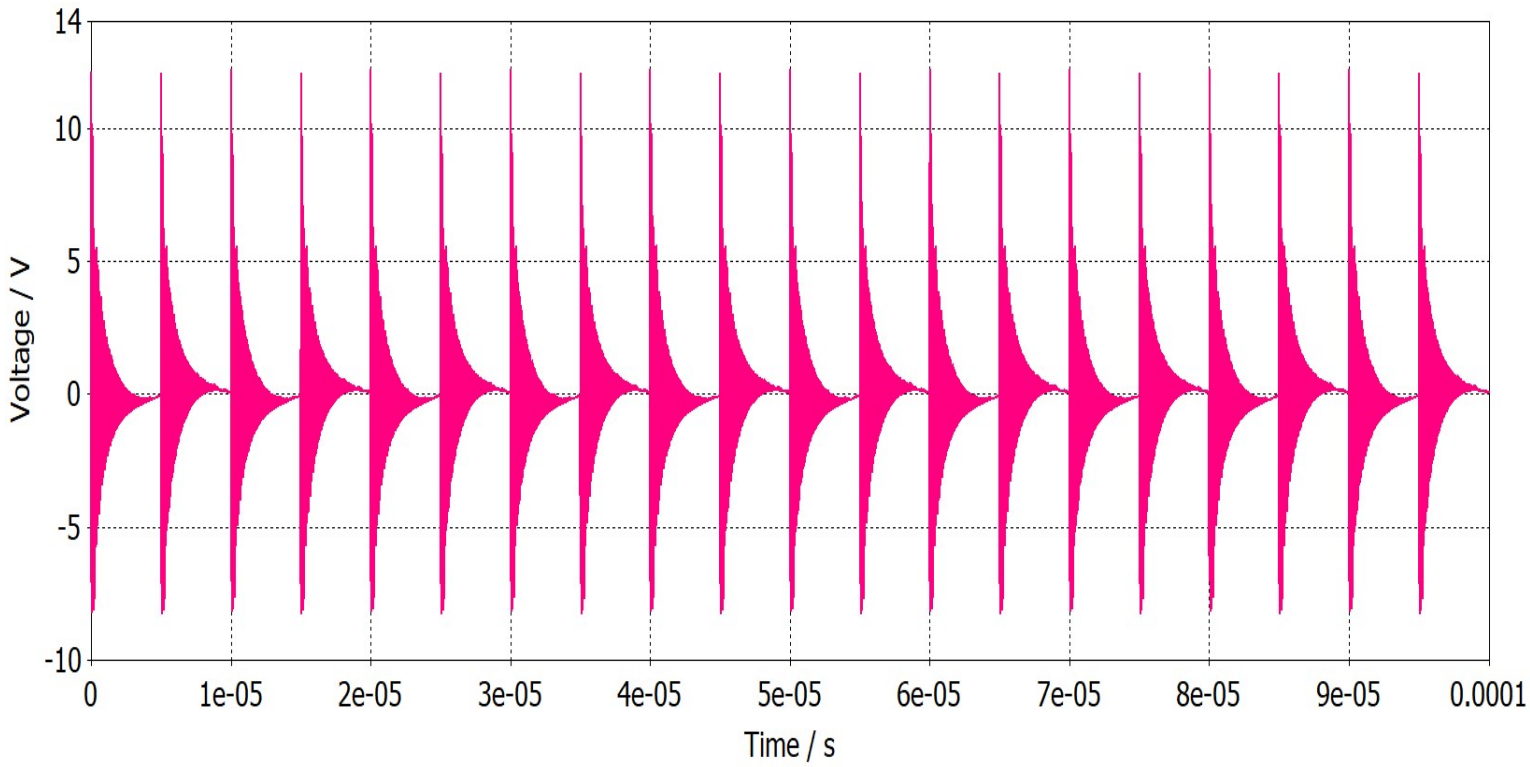

Figure 4.20: CST simulation with the interrupted shield - 1cm.

Chapter 5

CONCLUSION

The coupling mechanism between the HV cable and the adjacent signal cable in the DR was analyzed and its causes were validated. Shot noise (with a confirmed frequency of 10 MHz) occurs in the recovery diode of the HVG's secondary rectifier circuit. It has also been shown that the capacitive coupling is dominant and the noise problem can be solved simply with a decoupling capacitor. Although the result may change slightly depending on the braided shield parameters and the impedance of the receptor, the significance of this study resides in the analysis of shot noise.

Because the DR system is very complex and fully automated, it is susceptible to noise, and malfunctions caused by noise can cause injury to patients. In addition, if the X-ray exposure is not proper owing to noise problems, the number of unnecessary X-ray inspections may increase, and the radiation exposure will also increases. In the cases of medical devices, maintenance is important and reliability is essential.

As mentioned in the body sections, cable shielding is very effective in reducing EMI noise. It doesn't require a lot of time and effort like modifying the PCB, just replace to the shielded cable. For that reason, when an EMC problem occurs, cable shielding is the easiest and fastest solution. In particular, since it is difficult to determine the cause of noise problems in complex systems such as DR, cable shielding can be a good answer. However, shielding all cables is a cost burden and it is impossible.

So if it can be solved with one small passive element, it will be “Kill two birds with one stone.”

In the EMC area, know-how is a very important field because the problem patterns change according to the weather of the day and the situation on the site. In addition to it is not easy to match practical problems and theories. The noise and coupling mechanism that can occur in the DR system revealed in this study can provide good guidelines for the future DR system developers. I have no doubt that it will provide good debugging clues to EMC engineers. We believe that the role of EMC engineers is to suppress electromagnetic noise as much as possible at a minimum cost, improve product performance, but not lose reliability. We hope that this study will be helpful to other EMC engineers.

Bibliography

[1] IEC 60526:1978: High-voltage cable plug and socket connections for medical X-ray equipment, 2nd edition, 1978.

[2] H. W. Ott, *Electromagnetic Compatibility Engineering*, Wiley, New York, 2009.

[3] A. Tsaliovich, *Cable Shielding for Electromagnetic Compatibility*, Van Nostrand Reinhold, New York 1995.

[4] F. M. Tesche, *EMC Analysis Methods and Computational Models*, Wiley, New York 1995.

[5] E. F. Vance, "Shielding Effectiveness of Braided-Wire Shields," *IEEE Transactions on Electromagnetic Compatibility*, vol. EMC-17, no.2, pp. 71-77, May 1975.

[6] C. R. Paul, "Effect of Pigtails on Crosstalk to Braided-Shield Cables," *IEEE Transactions on Electromagnetic Compatibility*, vol. EMC-22, no.3, pp. 161-172, May 1980.

[7] C. R. Paul, "Symbolic Solution of the Multiconductor Transmission-Line Equations for Lines Containing Shielded Wires," *IEEE Transactions on Electromagnetic Compatibility*, vol. -33, no.3, pp. 149-162, August 1991.

[8] C. R. Paul, "Applications of multiconductor transmission line theory to the prediction of cable coupling-vol. Ⅲ-Prediction of crosstalk involving braided-shield

cables," Rome Air Development Center, Griffiss AFB, NY, Technical Report RADC-TR-76-101, 1980.

초 록

의료기기는 사람이나 동물에게 단독 또는 조합하여 사용되는 장치를 말하며 질병 예방, 진단 및 치료에 목적을 두고 있다는 점에서 타 전자제품과는 차이가 있다. 이 말은 단순히 성능적으로 우수하고 다양한 최신 기술이 적용되는 것이 중요한 게 아니라 얼마나 정확하고 신속히 진단을 내리고 치료를 할 수 있느냐가 핵심이라는 것이다. 물론 IT 업계에서 매년 쏟아져 나오는 최신 기술을 적용하는 것도 무시할 수 없지만 제품의 안정성, 신뢰성과는 또 다른 이야기이다.

Digital radiography (DR)는 수많은 회로와 cable, 전장부품들로 이루어진 시스템으로 규모가 크고 구조가 매우 복잡하여 전자기 장애 (EMI)로 인한 성능 저하나 타 전자기기에 피해를 줄 가능성을 많이 내포하고 있다. 특히 X-ray source 역할을 하는 high-voltage generator (HVG)로부터 발생하는 고전압 pulse는 DR 장비 전체로 퍼져 나가며 EMI 문제를 일으키고 오동작을 유발하곤 한다. 따라서 의료기기 제품에 있어 전자파 적합성 (EMC)은 곧 제품의 신뢰성과 직결된 분야이다.

본 프로젝트 리포트는 DR 시스템에 사용되는 HVG에서 발생하는 noise의 원인과 high-voltage cable을 경로로 인접 cable까지 coupling 되는 EMI noise에 대한 정도 및 저감 대책을 분석하였다.

High-voltage cable은 약 95%의 높은 optical coverage로 shielding 처리가 되어 있어 상당 부분의 EMI noise가 저감된다. 그러나 X-ray pulse의 크기는 수십 kV에 달하고 noise의 주파수 또한 낮지 않기 때문에 인접한 signal cable로 시스템 오동작을 유발할 만큼 충분한 수준으로 noise가 유입될 수 있다.

따라서 본 연구에서는 먼저 shielded cable에서 coupling이 발생하는 mechanism을 살펴보고 noise source의 경로 및 발생 원인, 그리고 등가회로 분석을 통한 coupling의 종류를 알아본다. 마지막으로 이에 대한 noise 저감 대책은 비용과 신뢰성 모두를 만족하게 할 방법을 제안한다.

주요어:Electromagnetic compatibility, Electromagnetic interference Digital radiography, Braided shield, Capacitive coupling, Inductive coupling, Crosstalk
학번: 2019-26941

ACKNOWLEGEMENT

가장 먼저 전기정보공학부 남상욱 교수님께 감사 드립니다. 삼성전자 학술 연수로 10년여 만에 다시 학업을 시작했을 때 느낀 감정은 초조함과 조바심 뿐이었습니다. 학부 수준의 이론조차 잊혔고, 당면한 이슈 해결에만 급급했던 현업에서의 경험들이 연구 활동에 있어는 오히려 장애 요소처럼 느껴지기도 했습니다. 학기 초부터 지나치게 조바심내던 제게 교수님 깨서는 서두르지 말고 기초부터 다시 차근차근 들여다보라고 조언해 주셨습니다. ”문제의 매커니즘을 정확히 이해하고 현상을 설명하지 못한다면 설령 해결했을 지라도 제대로 이해하고 있는 것이 아니다.”라고 여러 차례 일깨워 주셨고 덕분에 2년이라는 짧은 시간 동안 제가 생각했던 것보다 훨씬 많이 성장했음을 느낍니다. 더없이 훌륭하신 학자이자 스승이셨고 회사에 돌아가서도 받은 가르침 되새기며 더욱 더 좋은 엔지니어가 되어 보답하겠습니다.

전공 분야를 넘어 공학자로서의 시야를 넓혀 주신 공학전문대학원 김성우 교수님께도 감사의 인사 드립니다. 2년간 보여주신 넘치는 열정은 학생이자 엔지니어로서 저 자신을 돌이켜 보게 해주셨고, 사고의 틀을 넘어 생각하는 법을 가르쳐 주셨습니다. 항상 고민하고 도전하는 마음가짐으로 살겠습니다.

전파공학연구실에서 만난 인연들에도 감사합니다. 먼저 졸업한 선배들, 학교에 남아 있을 후배들 모두 좋은 동료이자 스승이었고 향후 사회라는 큰 바다에서 다시 만날 소중한 인연들임을 잊지 않겠습니다. 함께 보낸 2년이라는 시간이 우리 모두에게 좋은 자양분이 될 것을 믿어 의심치 않습니다.

사랑하는 어머니, 그리고 장인 · 장모님께도 감사드립니다. 부모님들의 사랑과

관심으로 성장 할 수 있었고, 심적으로 큰 지지대가 되어 주셨기에 학업 잘 마칠 수 있었습니다. 자랑스럽고 믿음직한 아들이자 사위가 되도록 노력하겠습니다.

끝으로 제 미래이자 현재인 사랑하는 아내 김지희와 아들들 박승연, 박호연에게 감사의 인사 전합니다. 그대들이야말로 제가 하루하루를 견뎌내게 해주는 힘의 원천이자 이유입니다. 제가 이뤄낸 모든 성과의 근본이고 세상 그 무엇보다 소중한 존재임을 짧은 글로나마 전합니다.

배움에는 끝이 없다고 합니다. 항상 학습하는 자세와 겸손한 마음가짐으로 살아가겠습니다. 감사합니다.